

Lawrence Berkeley National Laboratory

LBL Publications

Title

The Catalytic Manganese-Cluster: Organization of the Metal Ions", in
Photosystem II: The Light-Driven Water:Plastoquinone Oxidoreductase

Permalink

<https://escholarship.org/uc/item/0181c544>

Author

Yachandra, VK

Publication Date

2022-12-17

Peer reviewed

Chapter 10

The Catalytic Manganese-Cluster: Organization of the Metal Ions

Vittal K. Yachandra*

*Melvin Calvin Laboratory, Physical Biosciences Division, Lawrence Berkeley National Laboratory,
Berkeley, CA 94720, U.S.A.*

Summary	1
I. Introduction.....	2
II. Oxidation States of the Manganese	3
A. Mn X-ray Absorption Near Edge Spectroscopy (XANES).....	3
B. Mn K β X-ray Emission Spectroscopy (XES).....	3
C. Oxidation State Changes During S-State Transitions	5
1. S ₁ to S ₂ Transition	5
2. S ₀ to S ₁ Transition.....	6
3. S ₂ to S ₃ Transition.....	6
D. Summary of Oxidation State Assignments	7
III. Structure of the Mn Cluster	8
A. Heterogeneity in the Mn-Mn Distances and Structural Implications	10
B. S-State Transitions and Structural Changes.....	12
1. S ₁ to S ₂ (MLS) Transition.....	12
2. S ₁ to S ₂ (g=4.1) Transition.....	13
3. S ₂ to S ₃ Transition	13
4. S ₂ to S ₃ ' (S ₂ Y _Z ') Transition	14
5. S ₀ to S ₁ Transition	15
IV. Structural Role of the Calcium Cofactor	15
A. Mn Extended X-ray Absorption Fine Structure (EXAFS) and Ca.....	16
B. Sr Extended X-ray Absorption Fine Structure (EXAFS) and Ca	16
1. Isotropic Samples	16
2. Oriented Samples.....	16
3. Orientation of the Mn Complex.....	17
C. Ca Extended X-ray Absorption Fine Structure (EXAFS).....	17
V. Structural Role of the Chloride Cofactor.....	19
VI. Mechanism of Water Oxidation and O ₂ Evolution.....	20
Acknowledgments.....	22
References	22

Summary

The light-induced oxidation of water to O₂ is catalyzed by a four-manganese atom cluster associated with Photosystem II (PS II). This chapter summarizes ongoing investigations of the oxidation state, the structure and the associated cofactors calcium and chloride of the catalytic Mn cluster using X-ray and electron paramagnetic resonance (EPR) spectroscopy. Manganese K-edge X-ray spectroscopy, K β X-ray emission spectroscopy (XES), and extended X-ray absorption fine structure (EXAFS) studies have not only determined the oxida-

*Email: VKYachandra@LBL.gov

tion states and structural features, but also changes that occur in oxidation state of the Mn cluster and in its structural organization during the accumulation of oxidizing equivalents leading to O₂ formation. Combining X-ray spectroscopy information with X-ray diffraction studies, and consistent with the available EPR data, we have succeeded in limiting the range of likely structures of the Mn cluster. EXAFS studies at the strontium and calcium K-edges have provided evidence that the catalytic center is a Mn/Ca heteronuclear complex. Based on the X-ray spectroscopy data, models for the structure and a mechanism for O₂ evolution are presented.

I. Introduction

Most of the O₂ in the atmosphere that supports life on earth is generated by plants, algae, and cyanobacteria by the photo-induced oxidation of water to dioxygen:



This reaction is catalyzed by a manganese/calcium complex (Mn₄Ca), which sequentially stores four oxidizing equivalents (i.e. the S_n states, where n = 0 – 4) that are used to oxidize two molecules of water to molecular oxygen (Kok et al., 1970; for a review, see Joliot, 2003). The Mn complex is part of the multi-protein Photosystem II (PS II) assembly (Chapters 3–6), which contains the reaction center involved in photosynthetic charge separation (Chapter 7) and an antenna complex of chlorophyll molecules (Chapter 2). The assembly also contains cytochrome *b*₅₅₉ (Chapter 15) and a Fe-quinone electron acceptor complex (Chapter 8).

X-ray absorption spectroscopy (XAS) (Sauer et al., 1992; Robblee et al., 2001) and electron paramagnetic resonance (EPR) (Dismukes and Siderer, 1981; Messinger et al., 1997b; Britt et al., 2000) studies have emerged as the primary methods to provide structural and chemical information about the oxygen evolving complex (OEC) and devise a working model for its Mn cluster. XAS has been used to examine the structural environment of metal ions in many proteins (Cramer, 1988; Yachandra, 1995). The energy of the incoming X-ray photons and of the outgoing fluorescence is specific to the Mn atom;

Abbreviations: Chl – chlorophyll; <E> – 1st-moment value; EPR – electron paramagnetic resonance; EXAFS – extended X-ray absorption fine structure; FT – Fourier transform; IPE – inflection point energy; MLS – multiline EPR signal; Mn₄ – catalytic manganese cluster; OEC – oxygen evolving complex; PS II – Photosystem II; S_n – states of the OEC for n = 0, 1, 2, 3, or 4; XANES – X-ray absorption near edge spectroscopy; XAS – X-ray absorption spectroscopy; XES – X-ray emission spectroscopy; Y_D^{ox} – oxidized form of the redox active tyrosine on D2; Y_Z^{*} – oxidized form of the redox active tyrosine on D1

hence, other metals or the protein matrix normally co-purified with the OEC in a PS II preparation do not interfere. Element-specificity and applicability to non-crystalline samples have made X-ray spectroscopy a useful technique for probing the structure of the Mn complex in the complicated environment of PS II, which has many components such as non-heme iron, cytochrome, chlorophylls that interfere with other techniques. The structural studies can also be performed on crystals, or on frozen solutions and several of the S state intermediates mentioned above have been stabilized as frozen solutions and studied by X-ray spectroscopy. The different regions of the X-ray spectrum provide complementary information: X-ray absorption near edge spectroscopy (XANES) yield information about the oxidation states and site symmetry of the absorbing atom while extended X-ray absorption fine structure (EXAFS) is sensitive to distances, numbers, and atomic number of atoms around the absorbing atom. The more recently used technique of X-ray emission spectroscopy (XES) has also provided information regarding the identity of the oxidation states of Mn complex in the various S-states and the changes accompanying the S-state advance.

Critical questions related to the process of photosynthetic water oxidation are: (i) What are the oxidation state(s) and structural changes in the Mn complex as the OEC proceeds through the S-state cycle? and (ii) What is the mechanism by which four electrons are removed from two water molecules by the Mn complex to produce an O₂ molecule? Electron paramagnetic resonance (EPR) and X-ray spectroscopy studies and the interplay between these two methods have provided significant insights into the structure and the mechanism of the OEC. This chapter focuses on the application of X-ray spectroscopic techniques to resolve structural questions regarding the Mn cluster in the OEC, with emphasis on the results from our laboratory. Many excellent reviews are available for comprehensive surveys of the Mn complex and the OEC, EPR, and XAS literature (Debus, 1992; Rutherford et al., 1992; Britt, 1996;

1 Yachandra et al., 1996, 2002; Penner-Hahn, 1998;
2 Robblee et al., 2001).

3 4 5 **II. Oxidation States of the Manganese**

6
7 Two key questions for the understanding of photo-
8 synthetic water oxidation are: (i) do all four oxidiz-
9 ing equivalents necessary to oxidize water to O₂
10 accumulate on the four Mn ions of the OEC, or do
11 some ligand-centered oxidations take place before
12 the formation and release of O₂ during the S₃ → [S₄]
13 → S₀ transition; and (ii) what are the oxidation state
14 assignments for the Mn during S-state advancement.
15 X-ray absorption and emission spectroscopy of Mn,
16 along with EPR have provided answers to these two
17 pivotal questions.

18 19 **A. Mn X-ray Absorption Near Edge Spectros-** 20 **copy (XANES)**

21
22 X-ray absorption near-edge spectroscopy (XANES)
23 is the most well-known of the X-ray techniques and
24 has been extensively used to investigate the oxida-
25 tion states of redox-active metals in metalloprotein
26 active sites. XANES results from the excitation of a
27 1s electron (K-shell) to a higher, bound orbital (Fig.
28 1, *Left*). The higher the oxidation state of the metal,
29 the more positive the overall charge of the atom, and
30 higher energy is required to excite an electron out of
31 an orbital (Shulman et al., 1976). The first formally
32 allowed electric dipole transition is the 1s→4p tran-
33 sition. Due to the size of the 4p orbital, it overlaps
34 with p-orbitals of the ligands, either through σ or π
35 bonding. Consequently, this transition is sensitive
36 to the oxidation state and the ligand environment of
37 the metal. For certain symmetries around the metal,
38 the formally electric-dipole forbidden 1s→3d tran-
39 sition can be observed (arrow points to it in Fig. 1,
40 *Middle* which is expanded in the inset), occurring at
41 a lower energy than the main edge transitions (Roe
42 et al., 1984). This transition is due to mixing of metal
43 3d and 4p orbitals, and gives information about the
44 ligand as well as about the oxidation state and sym-
45 metry of the metal complex (Westre et al., 1997).
46 To increase the sensitivity of XANES, absorption is
47 detected as an excitation spectrum by measuring the
48 Kα fluorescence (2p to 1s) of the Mn atoms (Jaklevic
49 et al., 1977).

50 The pioneering application of Mn XANES to PS II
51 was performed by Kirby et al. (1981) on chloroplasts

52 and Goodin et al. (1984) on PS II preparations in the
53 early 1980s. These studies, although extremely dif-
54 ficult because of the low Mn concentration, showed
55 that the Mn K-edge from the S₂ state is shifted to
56 higher energy relative to the Mn K-edge from the S₁
57 state. Dramatic improvements in detector technology
58 and cryostat cooling capabilities have made XANES
59 experiments practical using concentrated PS II prepa-
60 rations (McDermott et al., 1988; Guiles et al., 1990a;
61 DeRose et al., 1994), and the collection of XANES
62 spectra from dilute, single-flash saturable PS II sam-
63 ples is now achievable. Three different groups have
64 investigated the oxidation states of Mn for the S₀, S₁,
65 S₂, and S₃ states using XANES on single-flash satu-
66 rable PS II samples. Based on shifts in the absorp-
67 tion edge, or lack thereof, Roelofs et al. (1996) pro-
68 posed that Mn is oxidized during the S₀ → S₁ and S₁ → S₂
69 transitions, but is not oxidized during the S₂ → S₃
70 transition. In contrast, Ono et al. (1992) and Iuzzolino
71 et al. (1998) interpret their XANES results to indicate
72 that Mn is oxidized during each S-state transition,
73 although Ono et al. (1992) reported no independent
74 S-state determination for their samples and Iuzzolino
75 et al. (1998) had significant S-state inhomogeneity
76 in their samples. However, improved XANES data
77 for S-state transitions, have shown a Mn K-edge shift
78 of only 0.4 eV for the S₂ to S₃ transition (Ono et al.,
79 1994). The results of Roelofs et al (1996) indicating
80 the absence of Mn centered oxidation during the S₂
81 to S₃ transition has been reproduced by Messinger
82 et al. (2001) using both XANES (Fig. 1, *Middle* and
83 *Right*) and Mn XES studies (see below).
84

85 86 **B. Mn Kβ X-ray Emission Spectroscopy (XES)**

87
88 The recent studies by Messinger et al. (2001) have
89 combined EPR, XANES and XES studies to ad-
90 dress the questions of oxidation state assignments
91 and changes during the S state cycle. In contrast to
92 XANES, Kβ XES detects the X-ray emission from
93 the relaxation of a 3p electron to a 1s hole, which is
94 created by excitation of a 1s electron into the con-
95 tinuum (Fig. 2, *Left*). In a simplified model, two final
96 states exist due to a constructive (Kβ_{1,3}) or destructive
97 (Kβ') spin-exchange interaction between the unpaired
98 electrons in the 3p and 3d orbitals (Tsutsumi et al.,
99 1976). The magnitude of the exchange interaction
100 depends on the number of unpaired electrons in
101 the 3d orbital. In the high spin case, increasing the
102 oxidation state of the metal decreases the number of
103 unpaired 3d electrons; concomitantly, the spin ex-
104

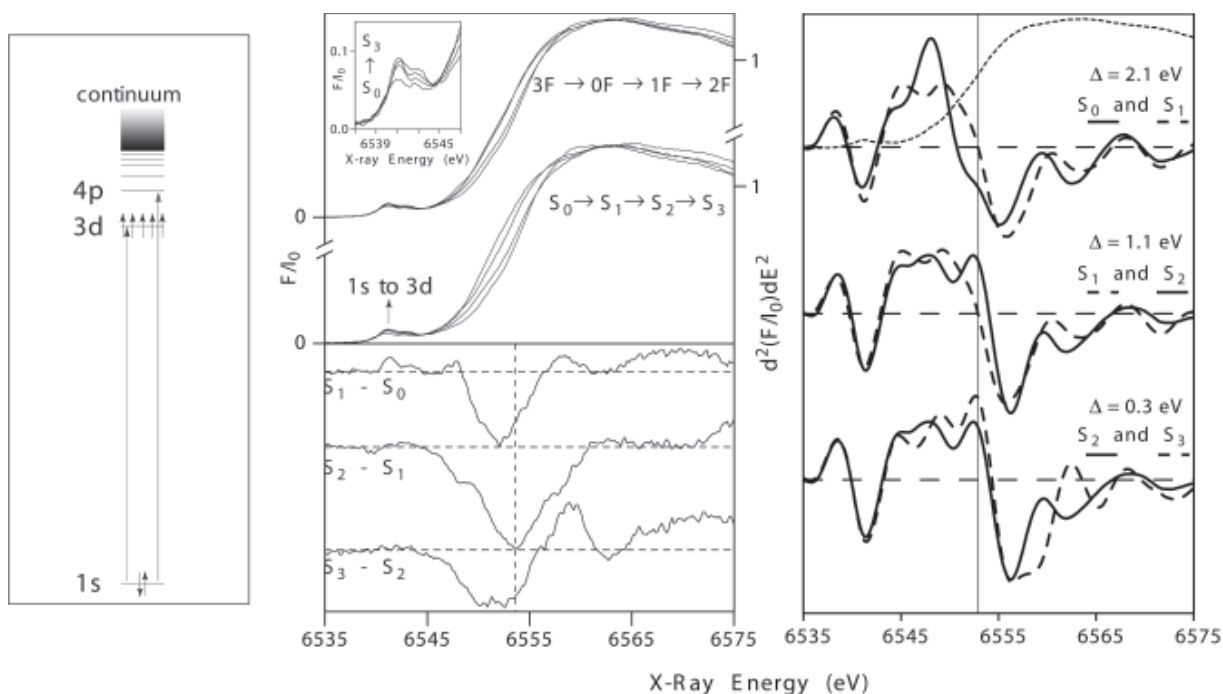


Fig. 1. *Left.* A schematic for the excitation and emission processes involved in Mn XANES. The weak 1s to 3d transition is dipole-forbidden and the principal transition is from 1s to a molecular orbital with p character. To enhance sensitivity, the X-ray absorption spectra are collected as excitation spectra using Mn K α (2p to 1s) fluorescence detection. *Middle Top.* Mn K-edge XANES spectra of flash-illuminated PS II samples. Pure S-state spectra (bottom) were obtained from the flash spectra (top) by deconvolution using multiline EPR spectra. The pre-edge region (principally a 1s \rightarrow 3d transition) for the S₀ – S₃ states is shown in the inset. The inflection point energy (IPE) changes from S₀ to S₁ and S₁ to S₂ transitions are substantial but are much smaller for the S₂ to S₃ transition. *Middle Bottom.* S-state Mn XANES difference spectra show that each transition is unique. The horizontal dashed lines show the zero value for each difference spectrum. Adapted from Messinger et al. (2001) and Visser et al. (2001). *Right.* Second derivatives of the normalized, pure S-state Mn K-edge spectra of the Mn-cluster of PS II. For clarity a vertical dashed line has been drawn at the inflection point energy (IPE) of the S₁-state. The change in IPE (Δ in eV) for each S-state advance is given at the right shows the significant shifts for the S₀ to S₁ and S₁ to S₂ transitions but is much smaller for the S₂ to S₃ transition indicating that a Mn centered oxidation is unlikely for the S₂ to S₃ transition. For reference, the K-edge spectrum of the S₁-state is plotted as well (dashed line). Adapted from Messinger et al. (2001).

change interaction decreases. Accordingly, the K $\beta_{1,3}$ transition shifts to a higher and the K β' transition shifts to a lower energy (Peng et al., 1994). Compared to the 4p orbitals, the 3p orbitals have less overlap with the ligand orbitals, because they are smaller and more buried within the electronic shells. Therefore, K β XES is less sensitive to the ligand environment compared to XANES. The K $\beta_{1,3}$ transition is better resolved than the K β' transition due to a difference in relaxation processes. Hence, the K $\beta_{1,3}$ transition is used as an indicator of the oxidation state of the metal. A more accurate view on K β XES requires the ligand-field multiplet formalism. This indicates that there is some dependence of the ligand environment on K β XES spectra.

Shown in Fig. 2, *Middle*, and inset are the K β emission spectra of Mn(IV)O₂, Mn₂(III)O₃, and Mn(II)O,

which illustrate the features of K β emission spectra and their sensitivity to the oxidation states of Mn. As the oxidation state of Mn increases from Mn(II) to Mn(III) to Mn(IV), fewer unpaired 3d valence electrons are available to interact with the 3p hole; thus, the magnitude of the 3p – 3d exchange interaction becomes smaller, leading to a decrease in the K β' – K $\beta_{1,3}$ splitting. The consequence is that, if one focuses only on the more intense K $\beta_{1,3}$ emission peak, it shifts to lower energy as Mn is oxidized. Whereas the K β emission spectrum is sensitive to oxidation state through a 3p – 3d exchange interaction, the technique of XANES spectroscopy is sensitive to oxidation state through a different mechanism: core-hole shielding effects. This is why, upon Mn oxidation, K $\beta_{1,3}$ emission spectra shift to lower energy, while XANES spectra shift to higher energy.

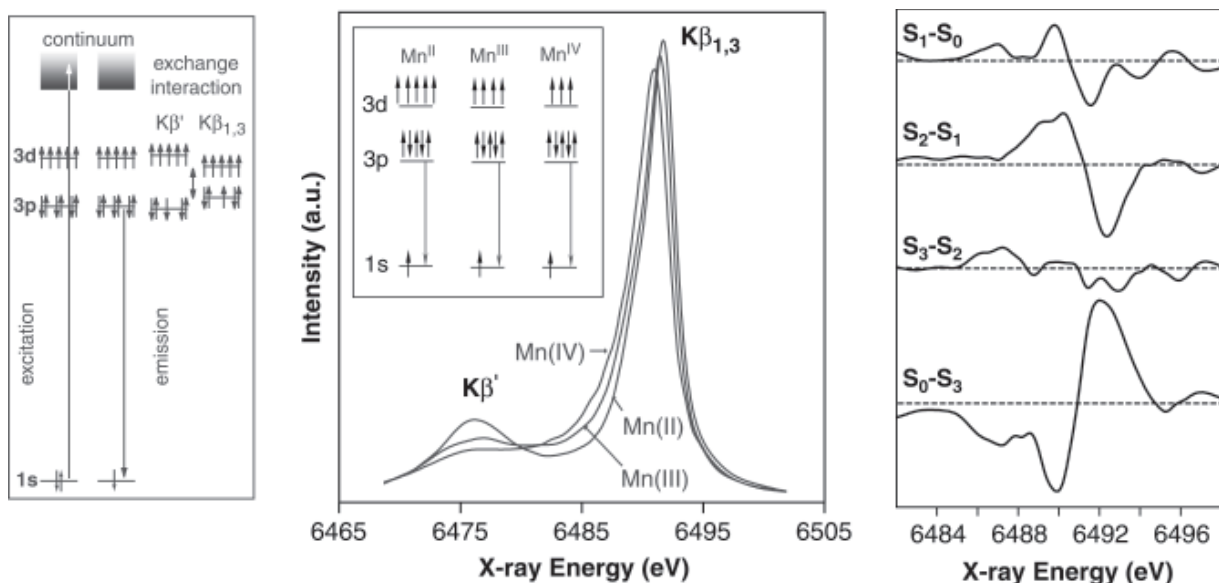


Fig. 2. K β spectra of Mn(II), (III) and (IV) oxides. *Left*. Energy level diagram showing the absorption (1s to continuum) and emission processes (3p to 1s) involved in K β Mn XES. In a simplified model, two final spin states exist with either a constructive (K $\beta_{1,3}$) or destructive (K β') spin exchange interaction between the unpaired 3p and 3d electrons. The magnitude of the interaction depends on the number of unpaired 3d electrons, which is related to the oxidation state of the metal. Adapted from Messinger et al. (2001) and Visser et al. (2001). *Middle*. Changes in the K β spectrum due to Mn oxidation. The inset shows a pictorial representation of the K β fluorescence transition for each of the oxides. K β XES arises from the emission of a 3p electron to 1s hole, which is formed following X-ray absorption. *Right*. The S₁-S₀, S₂-S₁, S₃-S₂ and S₀-S₃ difference high resolution Mn X-ray K β -emission spectra. The derivative shapes indicate shifts in the energy of the spectra between the S₀ and S₁, and S₁ and S₂ spectra, indicating oxidations of Mn. The S₃-S₂ difference spectra demonstrates the similarity of the spectra, suggesting that this advance does not involve a Mn centered oxidation. Adapted from Messinger et al. (2001).

Using a 1st-moment analysis, the position of the main K $\beta_{1,3}$ peak has been calculated for each S-state. Based on the shifts, or lack thereof, of the 1st moments ($\langle E \rangle$), it was concluded that Mn is oxidized during the S₀ to S₁ and S₁ to S₂ but not oxidized during the S₂ to S₃ transition. The results (shown as difference spectra in Fig. 2, *Right*) show a shift in energy between the S₀ and S₁ state spectra and between the S₁ and S₂ state spectra and seen in the derivative-shaped difference spectra. However, there is very little change between the S₂ and S₃ states, as seen in the difference spectrum (Messinger et al., 2001).

C. Oxidation State Changes During S-State Transitions

Besides determining whether Mn is oxidized or not during the S-state transitions, both XANES and XES also allow one to assign the oxidation states of the Mn atoms. This is often done by comparison to Mn model compounds.

1. S₁ to S₂ Transition

Mn K-edge XANES spectra (Fig. 1, *Middle* and *Right*) and the K $\beta_{1,3}$ emission spectra (Fig. 2, *Right*) indicate the presence of Mn oxidation from Mn₄(III₂,IV₂) to Mn₄(III,IV₃) during the S₁ to S₂ transition (Roelofs et al., 1996; Messinger et al., 2001), where the S₂ state is characterized by the multiline (MLS) or the g=4.1 EPR signal (Cole et al., 1987). This conclusion is corroborated by several other spectroscopic studies (Saygin and Witt, 1987; Kretschmann et al., 1988; Styring and Rutherford, 1988; Evelo et al., 1989; Dekker, 1992; Sharp, 1992) and is also confirmed by EPR spectroscopic measurements. S₂-state EPR multiline signal simulations (Hasegawa et al., 1998; Hasegawa et al., 1999) and ⁵⁵Mn ENDOR spectroscopy on the S₂ state (Peloquin et al., 2000) are most consistent with the oxidation states of Mn₄(III,IV₃); however, other simulations (Zheng and Dismukes, 1996) prefer oxidation states of Mn₄(III₃,IV) in the S₂ state.

If the S₂ state is proposed to be either in the

Mn₄(III,IV₃) or the Mn₄(III₃,IV) oxidation states, then the oxidation states of Mn in the S₁ state must be either Mn₄(III₂,IV₂) or Mn₄(III₄), which are both one-electron reductions from the oxidation-state proposals for the S₂ state. Although the oxidation state of Mn₄(III₄) for the S₁ state has been suggested by a few groups (Zheng and Dismukes, 1996; Kuzek and Pace, 2001; Chapter 12, Ahrling et al.), the XANES spectrum or its 2nd derivative of the S₁ state (Figs. 1 *Middle* and *Right*) shows that its edge shape is unlike the edge shape observed for Mn(III) complexes. When the XANES spectrum of the S₁ state, or its 2nd-derivative, is fit using Mn(III) and Mn(IV) model compounds, it cannot be fit well using only Mn(III) model compounds (Riggs et al., 1992; Yachandra et al., 1993). Furthermore, inspection of the only available set of tetranuclear Mn complexes with all O ligation, four distorted Mn₄(III₃,IV) cubanes, shows XANES inflection point energy (IPE) values at ~6551 eV for these complexes (Cinco et al., 1999) consistent with the S₀-state XANES IPE of 6550.8 eV and lower than the S₁-state XANES IPE of 6552.9 eV. These results are consistent with the conclusion that the oxidation states of Mn in the S₁ state are Mn₄(III₂,IV₂), not Mn₄(III₄).

An oxidation-state assignment of Mn₄(III₂,IV₂) is also consistent with recent Kβ XES experiments on the S₁ state. In fitting the Kβ_{1,3} emission spectrum for the S₁ state, Bergmann et al. (1998) found that the best fit to the experimental data was obtained using equal amounts of the Kβ_{1,3} emission spectra from Mn(III) and Mn(IV) model compounds; the fit was significantly worse if only Mn(III) or only Mn(IV) was used for the fit (Bergmann et al., 1998). It is therefore most likely that the oxidation states for Mn are Mn₄(III₂,IV₂) in the S₁ state and Mn₄(III,IV₃) in the S₂ state.

2. S₀ to S₁ Transition

The Mn K-edge XANES spectra for the S₀ to S₁ transition, displayed in Fig. 1, *Middle*, and the 2nd derivatives (Fig. 1, *Right*) show a clear shift of 2.1 eV (as determined by the 2nd-derivative IPE values) in the XANES edge position. In addition, the S₁/S₀ Kβ XES difference spectrum, shown in Fig. 2, *Right*, is derivative-shaped, which is indicative of Mn oxidation during this transition. Because the S₁ state has Mn oxidation states of Mn₄(III₂,IV₂), as detailed above, the changes in the X-ray spectroscopic data could be due to either a Mn(II) to Mn(III) oxidation or a

Mn(III) to Mn(IV) oxidation.

The finding that the S₁-S₀ XANES difference spectrum (Fig. 1, *Middle*) is somewhat different from the S₂-S₁ difference spectrum suggests that the S₀ to S₁ transition most likely reflects a Mn(II) to Mn(III) oxidation. The shape of the XANES edge is different for the S₀-state and S₁-state spectra; this is shown in part by the peak at 6548 eV in the 2nd derivative of the S₀-state XANES spectrum (Fig. 1, *Right*). This is suggestive of the presence of Mn(II), based on comparison to the 2nd derivatives of Mn(II)-containing model compounds. The significantly larger shift in the 2nd-derivative IPE values for the S₀ to S₁ transition compared to the S₁ to S₂ transition is also indicative for a Mn(II) to Mn(III) oxidation. This is based on the finding that, for homologous sets of model compounds, the shifts in the IPE value for Mn(II) to Mn(III) oxidations are usually larger than those seen for Mn(III) to Mn(IV) oxidations.

Other spectroscopic studies (Saygin and Witt, 1987; Kretschmann et al., 1988; Styring and Rutherford, 1988; Evelo et al., 1989; Guiles et al., 1990a; Dekker, 1992; Sharp, 1992; Messinger et al., 1997a,b; Åhring et al., 1998) concur that Mn oxidation occurs during the S₀ to S₁ transition. The greater spectral width of the S₀-state EPR multiline signal compared to the S₂-state EPR multiline signal has been attributed to the presence of Mn(II) in the S₀ state (Messinger et al., 1997a,b; Åhring et al., 1998), which suggests a Mn(II) to Mn(III) oxidation for the S₀ to S₁ transition. The presence of Mn(II) in the S₀ state may also explain why Y_D^{ox} can oxidize the S₀ state to the S₁ state, but not the S₁ state to the S₂ state.

The Kβ XES and XANES difference spectra, in addition to other spectroscopic data are consistent with the assignment of the S₀ to S₁ transition as a Mn(II) to Mn(III) oxidation. Therefore, the oxidation states of Mn in the S₀ state are proposed to be Mn₄(II,III,IV₂), which change upon Mn oxidation to Mn₄(III₂,IV₂) in the S₁ state, although the oxidation states of Mn₄(III₃,IV) for the S₀ state cannot be unequivocally excluded.

3. S₂ to S₃ Transition

The most controversial S-state transition has been the S₂ to S₃ transition. Most debate has focused on whether this transition is a Mn-centered (Ono et al., 1992; Iuzzolino et al., 1998) or ligand-centered (Guiles et al., 1990b; Roelofs et al., 1996; Messinger et al., 2001) oxidation. In addition, a redox isomerism

53
54
55
56
57
58
59
60
61
62
63
64
65
66
67
68
69
70
71
72
73
74
75
76
77
78
79
80
81
82
83
84
85
86
87
88
89
90
91
92
93
94
95
96
97
98
99
100
101
102
103
104

1 between Mn and ligands has been proposed for the
2 S_3 state (Renger, 1997). If Mn were to be oxidized
3 during the S_2 to S_3 transition, the oxidation would
4 have to be a Mn(III) to Mn(IV) transition. A Mn(IV)
5 to Mn(V) transition is unlikely to occur with Mn(III)
6 still present in the complex given the proposed re-
7 activity of the Mn(V) ion. Moreover, Mn(V) has a
8 very distinctive Mn XANES spectrum that has not
9 been observed in PS II preparations (V. Yachandra,
10 unpublished). Thus, it would be expected that the
11 XANES and $K\beta$ XES difference spectra, as well as
12 the observed shifts in the XANES IPE values and the
13 $K\beta$ emission spectra 1^{st} -moment values, $\langle E \rangle$, would
14 be essentially identical to the S_1 to S_2 transition, where
15 a Mn(III) to Mn(IV) oxidation also occurs. However,
16 as described below, the spectroscopic results for the
17 S_2 to S_3 transition are completely different from those
18 of the S_1 to S_2 transition.

19 The XANES results from Fig. 1 provide strong
20 support for a ligand-based oxidation of the OEC
21 occurring during the S_2 to S_3 transition, based on the
22 small (0.3 eV) shift in the XANES 2^{nd} -derivative IPE
23 values. The fact that the S_3 - S_2 XANES difference
24 spectrum is significantly different from the S_2 - S_1 dif-
25 ference spectrum (Fig. 1, *Middle*) is inconsistent with
26 a Mn(III) to Mn(IV) oxidation occurring during the
27 S_2 to S_3 transition. Instead, the S_3 - S_2 XANES dif-
28 ference spectrum shows how the shape of the XANES
29 edge changes between the S_2 and S_3 states, which is
30 consistent with a ligand-based oxidation.

31 Therefore, based on the XANES data, it is reason-
32 able to suggest that, a ligand radical is formed in the
33 S_3 state in lieu of Mn oxidation; this will be denoted
34 by $Mn_4(III,IV_3)$. This interpretation is reinforced by
35 the $K\beta$ emission spectra and especially, the $K\beta$ XES
36 difference spectra from Fig. 2, *Right*. The difference
37 spectra show that the derivative-shaped difference
38 spectrum that is expected if Mn is oxidized, as in the
39 S_0 to S_1 and S_1 to S_2 transitions, is absent in the S_2 to
40 S_3 transition. In addition, the $\langle E \rangle$ value of 6490.157
41 eV for the S_3 state argues against Mn oxidation dur-
42 ing the S_2 to S_3 transition, because it is inconsistent
43 with a $Mn_4(IV_4)$ oxidation state, which is required
44 for the S_3 state if Mn is oxidized during the S_2 to S_3
45 transition. Comparison of the S_3 -state $\langle E \rangle$ value to
46 the $\langle E \rangle$ values from 18 different monomeric, dimeric,
47 trimeric, and tetrameric Mn(IV) model compounds
48 with different ligands, including Cl⁻, shows that the
49 S_3 -state $\langle E \rangle$ value is higher than the $\langle E \rangle$ value for
50 any of the Mn(IV) compounds studied. It is difficult
51 to explain this result unless Mn(III) is still pres-

53 ent in the S_3 state, which means that, based on the
54 $Mn_4(III,IV_3)$ redox states derived for the S_2 state, a
55 Mn-based oxidation cannot occur during the S_2 to
56 S_3 transition. The EXAFS studies from the S_2 state
57 described below also support this assignment.
58

59 *D. Summary of Oxidation State Assignments*

60
61 The Mn K-edge energy and shape do not depend
62 solely on the oxidation state of the Mn atoms, but also
63 on the ligand environment. This is caused by mixing
64 of the ligand and the Mn atomic orbitals. It is possible
65 that a change in structure and ligand environment will
66 influence the main-edge energy and shape. Therefore,
67 care must be exercised when correlating the Mn K-
68 edge energies to Mn oxidation states without taking
69 into account the nature of the ligand environment.
70 This is especially a problem when sets of compounds
71 with different ligand structures, different nuclearities,
72 and different analysis methods to determine edge
73 positions are used to infer oxidation-state information
74 about biological systems, such as in Kuzek and Pace
75 (2001) and Carrell et al. (2002). However, numerous
76 studies have shown that there is a clear correlation
77 between Mn oxidation state and Mn K-edge energy
78 if the ligand environment stays the same, i.e. the IPE
79 shifts to a higher energy upon oxidation within sets
80 of homologous compounds.

81 A detailed XANES and XES study by Visser et
82 al. (2001) of homologous di- μ -oxo and mono- μ -oxo
83 bridged binuclear compounds in different oxidation
84 states shows that in contrast to Mn K-edge XANES,
85 $K\beta$ XES spectra show much less dependence on li-
86 gand environment. The shifts in XES spectra are the
87 same for a Mn(III) to Mn(IV) oxidation, irrespective
88 of whether the Mn is part of a di- or mono- μ -oxo
89 bridged structure (Visser et al., 2001). We have also
90 completed a XES study of homologous sets of tri- and
91 tetranuclear Mn compounds in different oxidation
92 states and we have found that the XES spectra are
93 much less dependent on the ligation or structure and
94 are primarily dependent on the oxidation state of Mn
95 (V. Yachandra, unpublished).

96 Considering both the limitations and strengths of
97 the two methods of XANES and XES, by comparison
98 with numerous Mn models and the knowledge from
99 EXAFS data (see below), we have proposed the oxida-
100 tion states shown in Fig. 3. Figure 3 summarizes the
101 $K\beta$ XES and XANES flash patterns from our most
102 recent and in our opinion the most comprehensive
103 study that leads to the conclusions about Mn oxidation
104

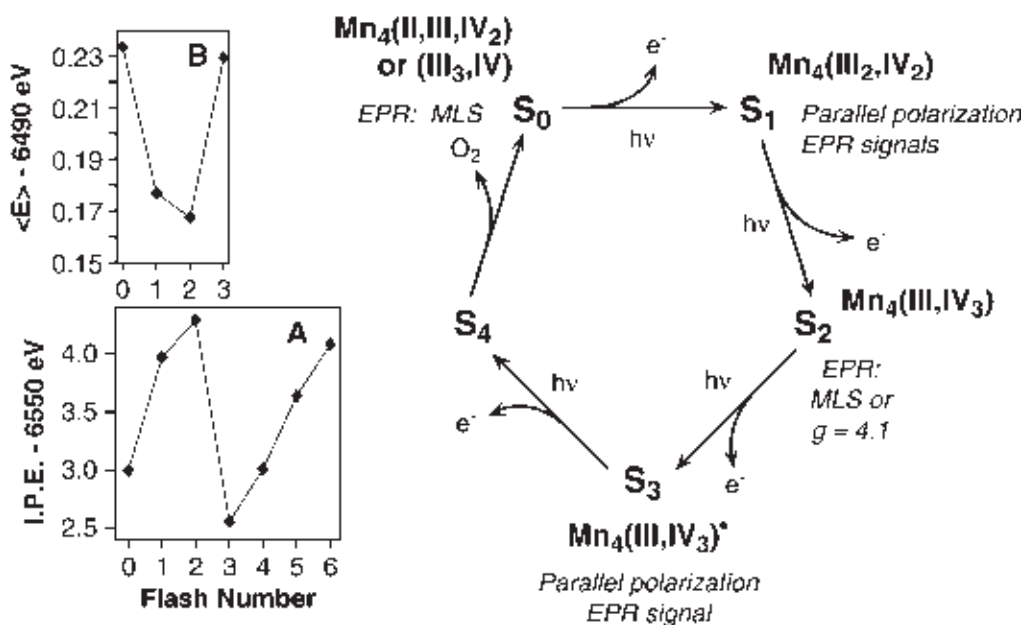


Fig. 3. Left. (A) Inflection-point energy (IPE) in eV of the Mn K-edge of PS II membranes as a function of the number of applied flashes. (B) The first moments of the Mn K β emission spectra ($\langle E \rangle$) as a function of flash number. The Mn K-edge shifts to higher energy as Mn is oxidized. The first moment of the Mn K β fluorescence shifts to lower energy as Mn is oxidized. The complementary and mutually reinforcing results provide a strong case for Mn oxidation during the S₀ to S₁ and S₁ to S₂ advances but no Mn-centered oxidation at the S₂ to S₃ advance. Right. The S-state scheme for O₂ evolution and the oxidation states that are consistent with the EPR signals and the X-ray absorption and emission spectroscopy results. Adapted from Messinger et al. (2001).

states. Both spectroscopies show a clear shift in the spectra to higher energy for XANES spectroscopy and lower energy for K β XES between the samples given 0 and 1 flashes indicating the presence of Mn oxidation during the S₁ to S₂ transition. The small change between samples given 1 and 2 flashes in both spectroscopies provides strong support for the S₂ to S₃ transition proceeding without a Mn-based oxidation. On the next transition, S₃ \rightarrow [S₄] \rightarrow S₀, O₂ is released, shifting the position of the spectra of samples given 3 flashes to lower energy for XANES spectroscopy and higher energy for K β XES. These flash patterns are explained by the proposed oxidation states of the Mn cluster in the S₀, S₁, S₂, and S₃ states, as shown. These oxidation states are: S₀: Mn₄(II,III,IV)₂ or Mn₄(III₃,IV), S₁: Mn₄(III₂,IV)₂, S₂: Mn₄(III,IV)₃, S₃: Mn₄(III,IV)₃*, where the superscript dot represents an oxidation that is not Mn centered.

III. Structure of the Mn Cluster

Extended X-ray absorption fine structure (EXAFS) spectra at the Mn K-edge results from the modulation

of the absorption cross section by the constructive and destructive interference of the 1s photoelectron wave with that backscattered from neighboring atoms (Sayers et al., 1971). The EXAFS modulations can be theoretically modeled to derive exquisitely detailed information about the distance from Mn to neighboring atoms to ~ 4 Å, often to an accuracy as precise as 0.015 Å (Yachandra, 1995). However, determination of the number of such interactions is susceptible to many uncertainties and can often be as large as 25%. The EXAFS approach has been used to determine the distances from Mn and identify the backscattering atoms of the Mn cluster present in the OEC. It is not possible to distinguish between O or N. But it is often facile to distinguish between light atoms such as N, or O, which are potential ligand atoms and backscattering from a heavier atom such as Mn or Ca that would only be present in a multi- or hetero-nuclear Mn complex. To interpret the results in terms of the coordination environment of the Mn, it has been necessary to examine a number of inorganic complexes of known structure, generously provided to us by our collaborators (Guiles et al., 1990a; DeRose et al., 1994; Cinco et al., 1999). The EXAFS

spectrum is usually presented as a Fourier transform (FT), which is similar to a radial distribution function with each Fourier peak representing shells of neighboring atoms from the absorbing atom. Dichroism resulting from oriented membranes can be used to derive information about the vectorial direction of the particular interaction. A typical Fourier transform from an S_1 state is shown in Fig. 4, *Top* (Yachandra et al., 1993; DeRose et al., 1994) and from oriented PS II membranes in the S_1 state in Fig 4, *Bottom* (Mukerji et al., 1994). Three distinct Fourier peaks are resolved in Fig. 4, *Top*, and dichroism is evident in all of the peaks in Fig. 4, *Bottom*.

On the basis of the latest findings, we conclude that each Mn is surrounded by a first coordination shell of O or N atoms at ~ 1.8 to ~ 2.1 Å (Fourier peak I), a set of Mn atoms at ~ 2.7 Å (Fourier peak II) and additional Mn and Ca at ~ 3.3 Å (Fourier peak III). Using model-compound data, it was straightforward to assign the two or three 2.7 to 2.8 Å Mn-Mn vectors to di- μ -oxo or hydroxo bridges between pairs of Mn atoms and the 3.3 Å Mn-Mn vector to one or two mono- μ -oxo bridged or similar longer interactions (Kirby et al., 1981; Yachandra et al., 1986, 1987; McDermott et al., 1988; George et al., 1989; Penner-Hahn et al., 1990; MacLachlan et al., 1992; DeRose et al., 1994; Mukerji et al., 1994; Kusunoki et al., 1995; Robblee et al., 2001). Furthermore, studies using Sr to replace Ca and, subsequently, direct measurements using Ca EXAFS, show unambiguously the presence of one or two 3.4 Å Mn-Ca vectors where the bridging motif could also be mono- μ -carboxylato or mono- μ -hydroxo (see below). The use of vector terminology to describe these interatomic interactions is particularly appropriate because of the direction information available from dichroism measurements on oriented samples. Furthermore, analysis of the EXAFS leads to the conclusion that the di- or mono- μ -oxo bridged Mn and Ca vectors are not co-linear; that is any three metal atoms in the cluster cannot be linear.

On the basis of such data many topological tetranuclear Mn structures (**A** through **K**) compatible with the observed EXAFS data have been presented (DeRose et al., 1994) (Fig. 5). These models have been described in detail (DeRose et al., 1994; Robblee et al., 2001). However, until recently only one of those options, **A**, was widely used as a working model, although options **E**, **F** and **G** (the nomenclature was initially introduced in DeRose et al. (1994)) have been shown to be preferred on the basis of EPR

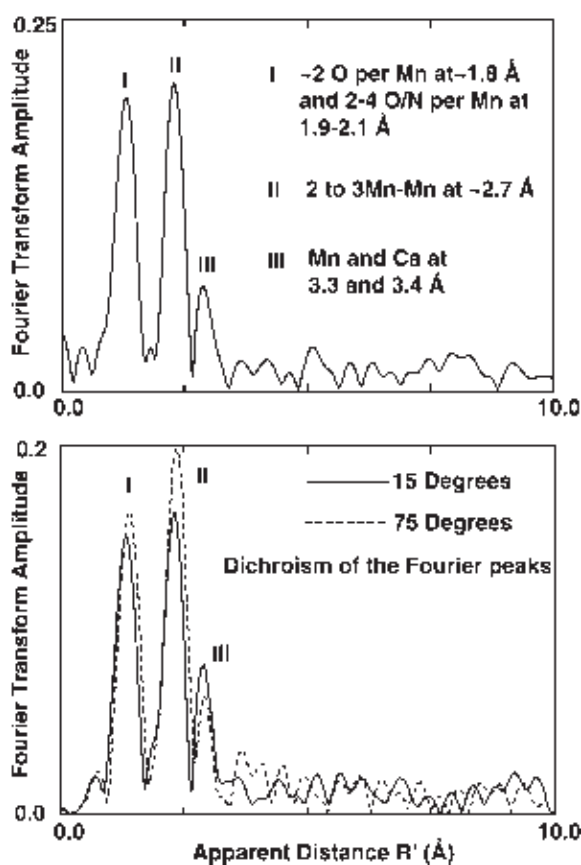


Fig. 4. Typical Fourier transform of the EXAFS spectrum from a S_1 state sample from an isotropic sample (*Top*) and oriented sample (*Bottom*). The three main Fourier peaks labeled I, II and III are assigned to ~ 2 O ligand atoms per Mn at 1.8 Å and 2-4 N/O ligand atoms per Mn at 1.9-2.1 Å (Fourier peak I), 2-3 Mn-Mn interactions at ~ 2.7 Å (Fourier peak II), and Mn and Ca at 3.3 and 3.4 Å (Fourier peak III), respectively. The dichroism of the Fourier peaks I, II and III is clear and can be used to determine the orientation of the vectors in the PS II membrane. Fourier peak II, that has been assigned to Mn-Mn interactions at ~ 2.7 Å, is maximal when the e-vector of the X-rays is parallel to the membrane plane (the angle on the figure is between the membrane normal and the X-ray e-vector). Adapted from Yachandra et al. (1993), DeRose et al. (1994) and Mukerji et al. (1994).

and ENDOR simulations (Hasegawa et al., 1999; Peloquin and Britt, 2001). Some of the structures, **A** through **K**, are less likely. Structure **C** and variations consisting of two isolated di- μ -oxo Mn-Mn moieties are preferred by Pace and co-workers based on their EPR simulations (Smith and Pace, 1996) but **C** is not widely accepted on the basis of EPR simulations by other groups (Boussac and Rutherford, 2000; Britt et al., 2000; Peloquin et al., 2000) or EXAFS data (Latimer et al., 1998). It is also physically impossible

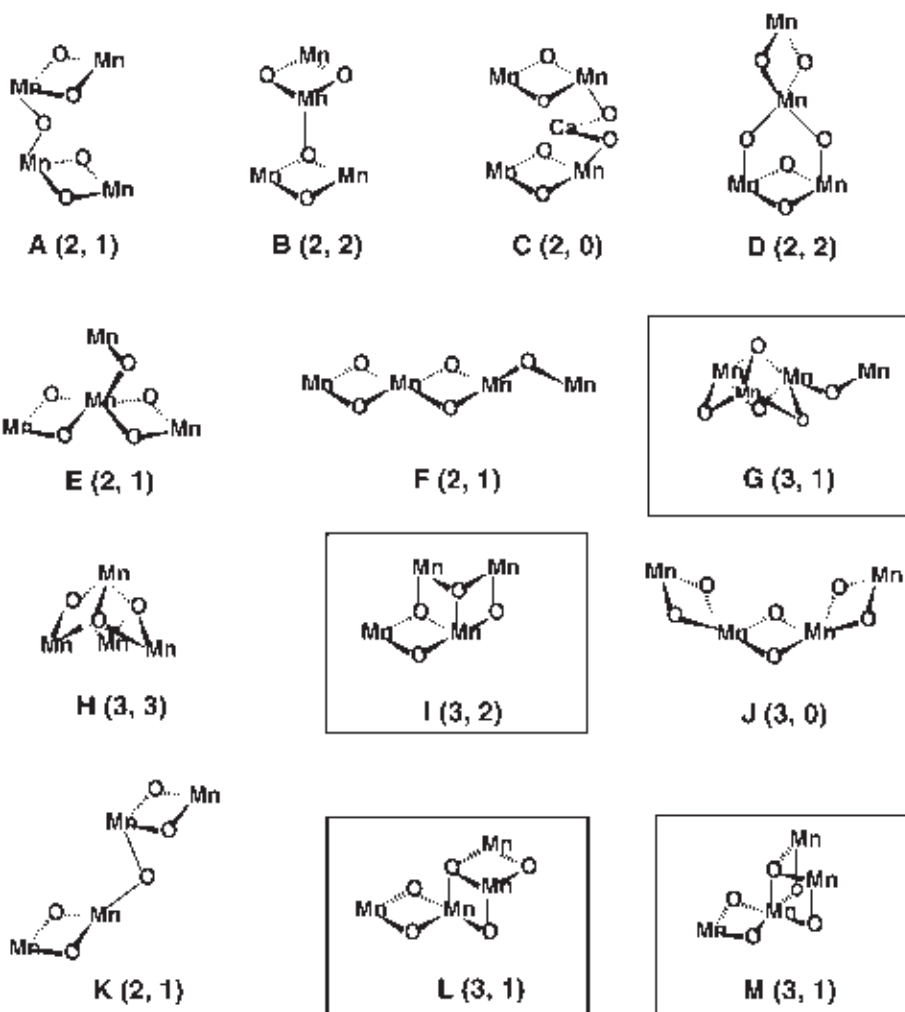


Fig. 5. Topological models for the Mn complex identified as compatible with the EXAFS data by DeRose et al. (1994) and Robblee et al. (2002). The numbers in parenthesis are the number of short 2.7 to 2.8 Å Mn-Mn vectors and long 3.3 to 3.4 Å Mn-Mn vectors. The options G, I, L and M all have 3 short 2.7 to 2.8 Å Mn-Mn vectors and are in better agreement with the X-ray diffraction studies; options E, F and G have been identified as compatible with EPR and ENDOR data. Option G or a topological isomer seems to be the best model by all presently available criteria; X-ray diffraction, EXAFS and EPR.

with four Mn atoms to obtain three Mn-Mn distances (see below) at 2.7 – 2.85 Å with two separated di- μ -oxo Mn-Mn moieties. Structure H, with three 3.3 Å Mn-Mn distances is unlikely, as shown by the EXAFS spectra from a similar set of complexes – a series of distorted cubanes (Cinco et al., 1999). The more likely candidates were considered to be A, E, F, G or K on the basis of EXAFS and EPR data; only G contained three Mn-Mn distances at \sim 2.7 Å, while the others had two such interactions.

A. Heterogeneity in the Mn-Mn Distances and Structural Implications

As mentioned above determining the number of Mn-backscattering atoms can be difficult. The number of the Mn-Mn 2.7 and 3.3 Å vectors (shown in parenthesis in Fig. 5) are especially important in this endeavor as these data directly lead or preclude certain arrangements of the Mn atoms that comprise the Mn cluster. The distance of the Mn-Mn vectors (at \sim 2.7 and 3.3 Å) is particularly important because it is easily the most reliably determinable parameter from the Mn EXAFS spectra of PS II. It is informative to focus on the \sim 2.7 Å Mn-Mn distance. When only one Mn-Mn 2.7 Å distance can be derived from the data as in the case of the S_1 and S_2 states, then one is constrained by

Table 1. Curve-fitting results for Fourier peak at ~ 2.7 Å that is characteristic of oxo-bridged Mn moieties from the S-states

S-state	Ref.	R_1 (Å)	R_2 (Å)	N_1	N_2	$N_1:N_2$
S_0^* state	Table III from Guiles et al. (1990a)	2.69	2.87	1.0	0.5	2:1
S_2 ($g = 4.1$) state	Table 4B from Liang et al. (1994)	2.72	2.85	0.76	0.44	1.7:1
NH_3 -inhibited S_2 state	Table 1 from Dau et al. (1995)	2.71	2.86	0.75	0.5	1.5:1
F-inhibited S_2 state	Table 2 from DeRose et al. (1995)	2.71	2.85	0.8	0.4	2:1
S_3 state	Table 1B from Liang et al. (2000)	2.82	2.95	0.7	0.4	1.8:1
S_0 state	Table 3 from Robblee et al. (2002)	2.72	2.86	1.05	0.46	2.3:1
S_0 state	Table 4 from Robblee et al. (2002)	2.72	2.85	1.02	0.51	2:1

N_1 and N_2 are the number of Mn-Mn interactions, normalized to one Mn in the Mn_4 complex, at the two distances R_1 and R_2 respectively. An N of 1 translates to two Mn-Mn distances and a N of 0.5 translates to 1 Mn-Mn distance at the corresponding distance. The $N_1:N_2$ ratio of 2:1 in the ~ 2.7 and ~ 2.8 Å Mn-Mn distances shows there are a total of 3 such short Mn-Mn distances in the OEC.

the uncertainty in the number of such interactions that is inherent to the EXAFS methodology; it is at present two or three such Mn-Mn interactions. However, when the distance degeneracy is lifted and there are two resolvable 2.7 or 2.8 Å Mn-Mn distances then one can determine the number of such vectors to a much higher accuracy because one can only have an integral number of each of such interactions.

Interestingly, when we examined states that exhibited such heterogeneity in the 2.7 Å Mn-Mn distances, it became quite clear that there was distinct preference for the existence of three such Mn-Mn vectors as described below (summarized in Table 1). Figure 6, *Left* shows the Fourier transforms (FT) of the k^3 -weighted EXAFS data from the S_0 and S_1 states. The Fourier peak II was isolated and fit to the EXAFS equation with one or two distances for the S_0 and S_1 states. Figure 6, *Right* shows the best fits to two Mn-Mn distances for the S_0 state as a function of the number of each of the Mn-Mn interactions. The contour plot graphically illustrates that the global minimum at two Mn-Mn interactions at ~ 2.7 Å and one Mn-Mn interaction at ~ 2.85 Å is very well defined (Robblee et al., 2002).

We have re-examined the data from the S_0^* (S_0 state induced by NH_2OH incubation), the $g=4.1$ S_2 , the NH_3 - or F-inhibited S_2 , and the S_3 states, where we have shown that there is distance heterogeneity in the Mn-Mn vectors. The results of this re-examination are given in Table 1, which show that none of the S-states that exhibit distance heterogeneity are best

fit by an equal N value for both Mn-Mn shells; the fit results from these S-states are in fact more consistent with a 2:1 $N_1:N_2$ ratio, where N_1 corresponds to the shorter distance. In each case, the ratio of the number of the two Mn-Mn interactions was $\sim 2:1$. This leads us to think that there may be three Mn interactions at ~ 2.7 Å in the Mn cluster in its native state, one of which is perturbed in the S_0 , F- and NH_3 -inhibited S_2 and the $g=4.1$ S_2 states, and all three are perturbed in the S_3 state.

On the basis of these re-evaluations of the results from the S_0 state and earlier data, it is important to consider the options that include three di- μ -oxo bridged moieties in the Mn cluster. Figure 5 shows several such options, **G**, **I**, and **J**, that were proposed earlier, and two newer options, **L** and **M**, among several others that can be conceived. Options **J** and **I** are less likely structures because **J** lacks a Mn-Mn interaction at 3.3 Å, and **I** has two such interactions. The EXAFS data from an inorganic compound (Auger et al., 1990) with the motif in option **J** is very different from that obtained from a PS II sample (V. Yachandra, unpublished). Options **G**, **L** and **M** all have three di- μ -oxo bridges and one mono- μ -oxo bridge; that is three 2.7 Å and one 3.3 Å Mn-Mn interactions. Options **L** and **M** are also similar to the structure proposed on the basis of density functional theory calculations although Ca is not included in **L** and **M** and is an integral part of the Siegbahn model (Siegbahn, 2000).

In addition to the constraints imposed by consider-

Note: when referring to unpublished data, the word "unpublished" stands alone; "data" or "results" are not added as this is not useful information.

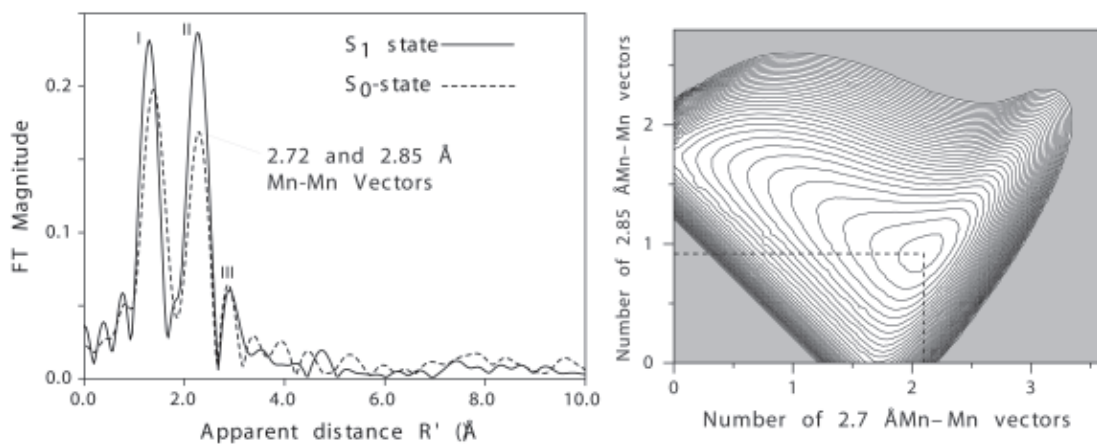


Fig. 6. Left. Fourier Transforms of the S_0 (dashed line) and S_1 state (solid line) of the Mn-EXAFS spectra. The main Fourier peaks are labeled I, II and III. There are clear differences in amplitude and position of these peaks between the S_0 and S_1 states. The peak labeled II is from Mn-Mn interactions at ~ 2.7 Å, and in the S_0 state this vector is best fit to two distances at 2.72 and 2.85 Å. Right. The contour plot shows the fit-quality-parameter ϵ^2 for the S_0 state plotted versus the number of the two Mn-Mn interactions. The dashed lines show the distinct minimum at one Mn-Mn vector at 2.85 Å and two Mn-Mn vectors at 2.7 Å. Adapted from (Robblee et al., 2002).

ing the EXAFS and EPR data, a preliminary structure of the OEC has been recently reported based on X-ray crystallographic data from PS II (Zouni et al., 2001; Kamiya and Shen, 2003; Ferreira et al., 2004; Chapters 19–21) and a further criterion for narrowing the choice of favored cluster geometries comes from these X-ray crystallography data of PS II. These data are most consistent with an OEC that is asymmetric and shaped somewhat like a ‘Y’. The arrangement of the Mn atoms has been described as pear-shaped (an elongated ellipsoid) with all four Mn lying approximately in the same plane. Presently, **G**, **L** and **M** are qualitatively in agreement with the asymmetry seen in the electron density of the Mn cluster (Zouni et al., 2001) and should be considered as possibilities for a topological model of the OEC based on the insights developed from the EXAFS spectroscopy results, with option **G** being the best in terms of being compatible with the most criteria; electron density, EPR, and EXAFS. However, as confirmed by Mn and Sr EXAFS studies (Latimer et al., 1995; Cinco et al., 1998) the OEC is most accurately described as a Mn/Ca heteronuclear cluster; therefore, Ca should be incorporated into each of the proposed structures so that 1–2 Mn–Ca vectors exist which are oriented close to the membrane normal (Ferreira et al., 2004; Chapter 21).

B. S-State Transitions and Structural Changes

Although EXAFS studies may not be able to uniquely identify the structure of the Mn complex, they are

invaluable in understanding the changes in structure, if any, that might be occurring during the S-state transitions. As noted above, EXAFS is exquisitely sensitive to distances of neighboring atoms from Mn and hence can provide a unique window into how the Mn cluster changes as it proceeds through the catalytic cycle, as summarized in Fig. 7. These changes in structure provide a rationale for testing various mechanisms that have been proposed as described below.

1. S_1 to S_2 (MLS) Transition

EXAFS studies of the S_1 state and the S_2 state characterized by the multiline EPR signal revealed that the Mn–Mn distances are essentially the same: ~ 2.7 Å and 3.3 Å in both states. This distance is consistent with those found in numerous studies of di- and mono- μ -oxo-bridged and $Mn_2(III,IV)$ and $Mn_2(IV,IV)$ complexes. Oxidation of a mono- or di- μ -oxo bridged Mn motif from (III,III) to (III,IV) or from (III,IV) to (IV,IV) has minimal effect on the Mn-Mn separation in many inorganic models (Wieghardt, 1989; Pecoraro, 1992; Pecoraro and Hsieh, 2000).

Interestingly, EXAFS studies on oriented PS II in the S_1 and S_2 states show that there may be heterogeneity in the 2.7 Å vector, a contention that is supported by related studies on modified S_2 states. This Mn-Mn vector has been determined to be at an average angle of $\sim 60^\circ$ to the membrane normal (Mukerji et al., 1994; Dau et al., 1995).

Note: the "new" Fig. 6 sent on the disk with the corrected 1st proof does not contain the dashed line indicated by the author. No version of this figure that I have received contains this dashed line.

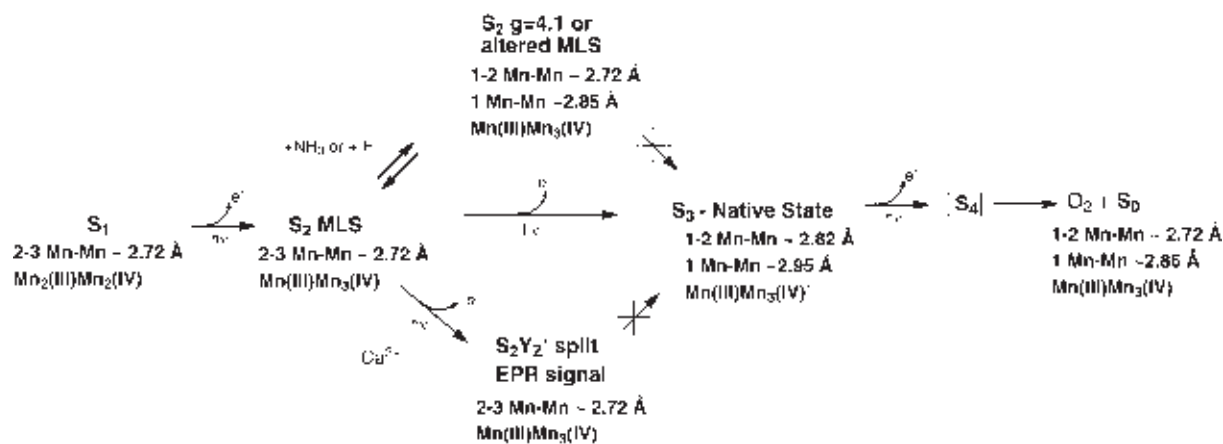


Fig. 7. Summary of the changes in oxidation states and Mn-Mn distances at 2.7 to 3.0 Å in the native S_1 , native S_2 , modified S_2 , S_3^* ($S_2 Y_Z^*$), native S_3 and S_0 states of PS II as determined by Mn EXAFS.

2. S_1 to S_2 ($g=4.1$) Transition

The inequivalence of the di- μ -oxo bridged Mn units becomes more evident in the S_2 state that is prepared by illumination at 130 K and characterized by the $g=4.1$ EPR signal (Liang et al., 1994). Similar results were obtained with NH_3 -treated and annealed S_2 state samples (Dau et al., 1995) and in F^- -treated samples (DeRose et al., 1995). The scheme in Fig. 7 shows that there are paths from the MLS S_2 state that lead to two states: the S_2 - $g=4.1$ state inhibited by NH_3/F^- or the $S_2 Y_Z^*$ states; neither of these states can proceed to the physiologically relevant S_3 state. These states are depicted in Fig. 7 as branching away from the normal pathway leading to the S_3 state by photon absorption. However, the S_2 - $g=4.1$ state generated by 820 nm illumination at 130 K (Boussac et al., 1996) can proceed to an S_3 state (Zimmermann and Rutherford, 1986). In the modified S_2 states, one of the Mn-Mn distances increases to ~ 2.85 Å, whereas there is very little change in the other one or two 2.7 Å or the 3.3 Å Mn-Mn distance. With the degeneracy of the 2.7 Å lifted, it has been possible by studying the dichroism of the Fourier peak, to assign the relative orientation of the 2.7 and 2.85 Å vectors (Dau et al., 1995), which are oriented at 55° and 67° respectively to the membrane normal.

The NH_3 -treated and F^- -treated samples cannot advance beyond the modified S_2 state ($S_2 Y_Z^*$ state). It is likely that F^- or NH_3 prevent the oxidation of a ligand atom, thereby blocking structural changes from occurring that are necessary for the formation of the S_3 state, and thus inhibiting O_2 evolution

activity. In the case of NH_3 , it is probably due to an amido-group (NH_2^-) replacement of the oxo-bridge involved in oxidation. The modification of the MLS spectra upon addition of NH_3 (Beck et al., 1986) and ESEEM studies using $^{14}NH_3$ and $^{15}NH_3$ demonstrated that NH_3 becomes a ligand of Mn (Britt et al., 1989). The asymmetry parameter derived from ESEEM results suggested that the amido group is likely to be a bridging ligand (Britt et al., 1989). It is probable that the oxo-bridge that is displaced by NH_3 is oxidized during the S_2 to S_3 transition (see next section).

3. S_2 to S_3 Transition

Earlier XAS data from the S_3 state samples produced by a cryogenic double-turnover method indicated increased disorder in the peak at 2.7 Å; that a structural change that involved the lengthening of the Mn-Mn distance was occurring between the S_2 and S_3 states and was absent during the S_1 to S_2 state transition (Guiles et al., 1990b). More recent detailed analysis of data from native S_3 state samples created under physiological conditions with saturating actinic flash illumination show there is a significant change in the 2.7 Å Mn-Mn distances that characterize the di- μ -oxo bridged Mn-Mn; with an increase in the short Mn-Mn distances from 2.7 Å to ~ 2.8 and ~ 3.0 Å (Liang et al., 2000).

The perturbation in the Mn-Mn distances is different from that observed in the modified S_2 states. Each of the altered S_2 states gives a fit that is consistent with the alteration of one of the Mn-Mn distances from ~ 2.72 to 2.85 Å. Unlike the modified S_2 states,

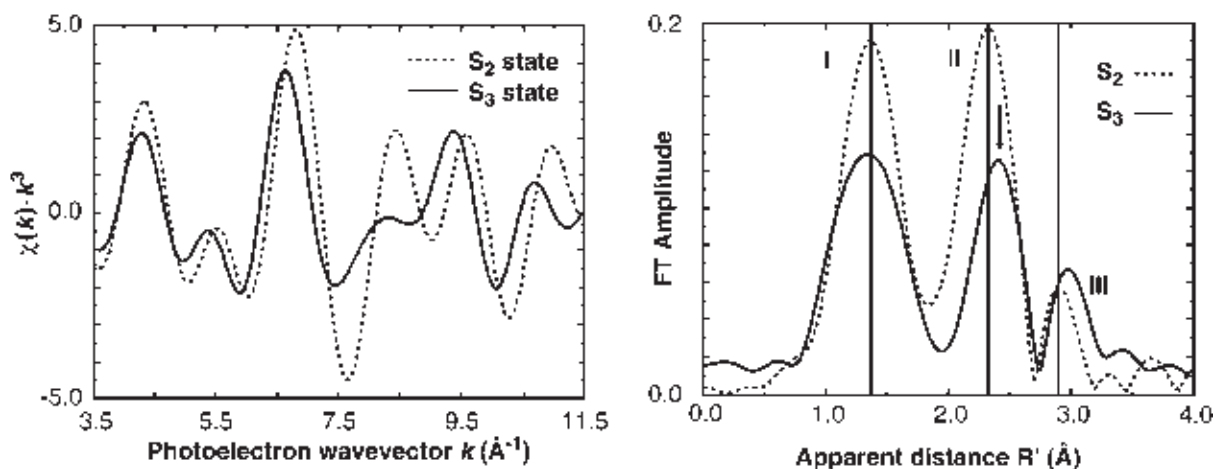


Fig. 8. Left. Fourier-filtered k -space EXAFS data from S_2 (dashed line) and S_3 (solid line) state of PS II samples. The differences in phase, frequency and amplitudes between the raw S_2 and S_3 state EXAFS spectra are very obvious in these spectra. Right. Fourier transform power spectra of S_2 (dashed line) and S_3 (solid line) states of PS II. The major Fourier peaks are labeled I, II and III. The spectra are clearly different between the S_2 and S_3 states. There is a reduction in amplitude in all three peaks in the S_3 state compared to the S_2 state. More importantly, peaks II and III are at a greater apparent distance R' for the S_3 state compared to the S_2 state as shown.

the position of Fourier peak II from the native S_3 state clearly shifts to a longer distance in the FTs (Fig. 8) with one or two Mn-Mn distances of 2.82 \AA and one Mn-Mn distance of 2.95 \AA (Liang et al., 2000). These results underscore the point that during the S_2 to S_3 transition under physiological conditions, *all* of the di- μ -oxo-bridged Mn-Mn units undergo structural changes that lead to an increase in the Mn-Mn distances. A change in the Mn-Mn distance from 2.7 to 3.0 \AA was also observed in samples that had been depleted of Ca by NaCl treatment (MacLachlan et al., 1994). The best fits for the Mn-O/N shell shorter Mn-O distance is characteristic of Mn-O bridging distances and it increases from 1.80 \AA in the S_2 state to 1.86 \AA in the S_3 state. This is a significant change, and it provides additional evidence for the involvement of the bridging oxygen atoms during the S_2 to S_3 transition.

The results from isotropic S_3 samples are supported by polarized EXAFS studies on oriented PS II in the native S_3 state. The data confirm that the two Mn-Mn vectors units are not equivalent. The polarized EXAFS data are different from those observed in the S_2 state (Mukerji et al., 1994; Dau et al., 1995). Fourier peak II of S_3 is dichroic and is readily resolved to Mn-Mn distances of ~ 2.8 \AA and ~ 3.0 \AA , each with its own distinct projection on the membrane normal (Fernandez et al., 1998). Schiller et al. (1998) have reported results on the oriented S_3 state, showing an increase in the amplitude of Fourier peak II that is

interpreted as an increase in the number of 2.7 \AA Mn-Mn interactions in the S_3 state. However, a closer examination of their FTs indicates that Fourier peak II occurs at a longer distance and is broader compared to that in the S_2 state.

In the S_3 state it is seen that Fourier peak III at ~ 3.3 \AA occurs at a greater apparent distance than that of the S_2 state indicating a lengthening of the two Mn-Mn distances or the Mn-Mn and Mn-Ca distances compared to the S_2 state by 0.04-0.2 \AA .

Significant changes are observed in the Mn-Mn distances in the S_3 state compared to the S_1 and the S_2 states (Fig. 8). These changes in Mn-Mn distances are interpreted as consequences of the onset of substrate water oxidation in the S_3 state. Mn-centered oxidation is evident during the S_0 to S_1 and S_1 to S_2 transitions. During the S_2 to S_3 transition, we propose that the changes in Mn-Mn distances are the result of ligand or water oxidation, leading to the formation of an oxyl radical intermediate formed at a bridging or terminal position. The reaction of the oxyl radical with OH^- , H_2O , or an oxo group during the subsequent S-state conversion is proposed to lead to the formation of the O-O bond (Chapter 25).

4. S_2 to S_3' ($S_2Y_Z^*$) Transition

The other unproductive state generated from the S_2 -MLS state is denoted in Fig. 7 as the S_3' state or $S_2Y_Z^*$ state generated in Ca-depleted samples. The

1 Ca-depleted samples are inactive in O₂ evolution,
2 while a broad $g = 2$ EPR signal has been observed
3 in such samples. The $g = 2$ broadened EPR signal
4 has been confirmed to arise from the tyrosine Y_Z
5 radical (Gilchrist et al., 1995; Peloquin et al., 1998)
6 and it is proposed that the signal is broadened by
7 interaction with the spin on the Mn cluster (Lakshmi
8 et al., 1998).

9 EXAFS analysis from Ca-depleted S₃' state
10 samples (S₂Y_Z') (Latimer et al., 1998) shows that
11 Fourier peak II (Mn-Mn distance of ~2.7 Å) in the
12 FT of S₃' state samples (S₂Y_Z') was invariant relative
13 to that of the native S₂ state sample. The EXAFS fits
14 showed that the ~2.7 Å Mn-Mn distances did not
15 lengthen as observed in the native S₃ state samples
16 and are essentially unchanged from those of the na-
17 tive S₂ state. This finding is surprising because the
18 Mn K-edges from these Ca-depleted samples showed
19 a behavior similar to the native PS II in that little
20 or no shift was observed in the S₂' to S₃' (or S₂Y_Z')
21 transition. This difference between the native S₃ and
22 Ca-depleted S₃' states indicate that the core di-μ-oxo-
23 bridged structure is probably dissimilar in the native
24 S₃ and the S₃' (S₂Y_Z') states, with the structure in the
25 S₂Y_Z' state resembling the native S₂ state structure.
26 It is intriguing how the transfer of one electron from
27 the Mn cluster onto Y_Z result in major changes in
28 the Mn-Mn distances as is observed in the native S₃
29 state. The roles of the Y_Z and the Mn cluster in the
30 process of water oxidation are clearly delineated by
31 the comparison of the S₃ and the S₃' (or S₂Y_Z') states.
32 Instead of the Mn cluster just providing a scaffolding
33 for water oxidation, this comparison shows that the
34 structural change in the Mn cluster initiated by the
35 transfer of an electron from the Mn cluster to Y_Z dur-
36 ing the S₂ to S₃ transition might provide the trigger
37 to the chemistry of the formation of the O-O bond,
38 via the formation of a ligand radical. The results
39 show that the Mn cluster is involved in a much more
40 intimate manner in the catalysis than just providing
41 the framework. The implications to the mechanism
42 are significant (Chapter 25).

43 In Ca-depleted systems the tyrosine Y_Z radical
44 is stabilized and the oxidation of the Mn-OEC and
45 the concomitant changes in Mn-Mn distances are
46 prevented. In the S₃ state, with Ca present, the oxida-
47 tion equivalent resides on the Mn cluster leading to
48 profound changes in the Mn-Mn distances. Thus, Ca
49 is proposed to play a crucial role in controlling the
50 redox potential and thus the course of the mechanism
51 of water oxidation.

5. S₀ to S₁ Transition

53
54
55 Early EXAFS experiments by Guiles et al. (1990a)
56 with the S₀ state used chemical treatments to get
57 around the problem of low concentrations. However,
58 the S₀ state generated in this manner was designated
59 as S₀* to emphasize that it is generated through
60 chemical treatment and is thus not a native S-state.
61 Although hampered by a low signal-to-noise ratio and
62 the uncertainty about the relationship between the
63 chemically generated S₀* state and the native S₀ state,
64 those experiments provided the first evidence from
65 EXAFS that heterogeneity may exist in the 2.7 Å
66 Mn-Mn distances in the S₀ state in the form of a
67 reduced amplitude of Fourier peak II in the S₀* state
68 relative to that in the S₁ state.

69 Riggs-Gelasco et al. (1996a) examined reduced
70 S states of the OEC generated by treatment with
71 NH₂OH or hydroquinone and observed a decrease
72 in the amplitude of the 2.7 Å Mn-Mn Fourier peak.
73 This was interpreted as a reduction in the number of
74 Mn-Mn vectors instead of the appearance of distance
75 heterogeneity.

76 Recent EXAFS experiments by Robblee et al.
77 (2002) show that, in the S₀ state, heterogeneity most
78 likely exists in the 2.7 Å Mn-Mn distances with one
79 or two Mn-Mn distances at 2.72 Å and one Mn-Mn
80 distance at 2.85 Å (as described above, see Fig. 6),
81 which can be explained through the protonation of a
82 di-μ-oxo-bridged Mn-Mn moiety and/or the presence
83 of Mn(II) (Chapter 25). The presence of distance
84 heterogeneity in the S₀ state has been exploited in
85 the curve-fitting procedure, whose results are sug-
86 gestive of the possibility that three di-μ-oxo-bridged
87 Mn-Mn moieties may exist in the OEC instead of
88 the two di-μ-oxo-bridged Mn-Mn moieties that are
89 widely used in proposed structural models for the
90 OEC (see above).

IV. Structural Role of the Calcium Cofactor

94
95 Along with Mn and Cl⁻, Ca is an essential cofactor in
96 O₂ evolution (Debus, 1992; Chapter 13, van Gorkom
97 and Yocum). Depleting this cofactor suppresses
98 OEC activity, which can be restored (up to 90%) by
99 replenishing with Ca²⁺. Partial reactivation (up to
100 40%) results from addition of Sr²⁺ to Ca-depleted
101 PS II membranes (Ghanotakis et al., 1984; Bous-
102 sac and Rutherford, 1988b) and no other metal ions
103 can restore activity, making this requirement highly
104

1 specific for Ca or Sr (Ghanotakis et al., 1985; Ono
2 and Inoue, 1989).

3 Although Sr²⁺ replenishes the Ca-depleted centers
4 to a similar extent as added Ca²⁺, the slower kinetics
5 of the OEC turnover yields an overall lower steady-
6 state rate (Boussac and Rutherford, 1988a) (40%) at
7 saturating light intensities. Substitution of Ca with
8 Sr also alters the EPR multiline signal (MLS) from
9 the S₂ state, giving narrower hyperfine splitting and
10 different intensity patterns (Boussac and Rutherford,
11 1988b; Sivaraja et al., 1989). Most researchers ad-
12 dressing the stoichiometry of the Ca cofactor in PS II
13 now conclude that functional water oxidase activity
14 requires one essential Ca²⁺, which can be removed
15 by low-pH/citrate or 1.2 M NaCl wash (Cammarata
16 and Cheniae, 1987; Katoh et al., 1987; Ono and In-
17 oue, 1988; Shen et al., 1988; Adelroth et al., 1995).
18 In higher plants, another more tightly bound Ca is
19 associated with the light-harvesting complex (LHC
20 II) and requires harsher treatments for its removal
21 (Han and Katoh, 1993; Chen et al., 1995).

22 *A. Mn Extended X-ray Absorption Fine Struc-* 23 *ture (EXAFS) and Ca*

24 Several investigations have involved removal of Ca
25 and substitution of various metals into this binding
26 site, followed by EXAFS studies on the Mn cluster.
27 One set of experiments using Mn EXAFS on Sr-reac-
28 tivated PS II membranes was interpreted to indicate
29 a 3.4–3.5 Å distance between the Ca (Sr) and the Mn
30 cluster (Latimer et al., 1995). This conclusion was
31 based on the observation of increased amplitude in
32 Fourier peak III at 3.3 Å upon replacement of Ca with
33 Sr, a heavier atom and better X-ray scatterer. Analysis
34 of EXAFS spectra from purified PS II membrane
35 preparations indicated a Mn–Ca interaction at slightly
36 longer distance (MacLachlan et al., 1992) (~3.6–3.7
37 Å). Ca depletion by NaCl-washing of PS II mem-
38 branes removed the 16 and 23 kDa extrinsic proteins
39 and led to a reduced amplitude for this 3.6 Å feature
40 and because of the lower X-ray scattering ability of
41 Na, this result was interpreted as possible Na⁺ sub-
42 stitution for Ca²⁺ at this distance (MacLachlan et al.,
43 1994). Another Mn EXAFS study (Riggs-Gelasco et
44 al., 1996b) did not detect any changes in the Fourier
45 peak at 3.3 Å when Ca was replaced with Sr²⁺ or
46 Dy³⁺ in PS II reaction center complexes lacking the
47 16 and 23 kDa extrinsic polypeptides; however, it
48 was proposed that Ca might be linked via a hydrogen
49 bond to the oxo ligand of the Mn cluster.
50
51
52

B. Sr Extended X-ray Absorption Fine Struc- 53 *ture (EXAFS) and Ca*

1. Isotropic Samples

54
55
56
57
58 The most common approach, as described above
59 (Latimer et al., 1995; Riggs-Gelasco et al., 1996b),
60 was to substitute other metals (such as Sr) for Ca
61 and then use Mn EXAFS to detect changes in the
62 cluster. Isolating the Mn-Ca or Sr component of
63 the EXAFS spectrum from the combined EXAFS
64 from all Mn-ligand and Mn-Mn interactions can be
65 difficult. The reverse experiment where one probes
66 for backscattering from Mn using Ca or Sr EXAFS
67 (Ca/Sr cofactor point-of-view for nearby Mn) is an
68 elegant alternative and is more definitive than Mn
69 EXAFS results. Such studies on both isotropic and
70 oriented PS II membranes have yielded unequivocal
71 evidence for the proximity of Ca to the Mn cluster
72 (see below).

73 Several factors favor Sr as the better cofactor
74 for XAS study. First, the X-ray energies involved
75 (16 keV for the K-edge) are more penetrating and
76 not attenuated by air. The higher X-ray absorption
77 cross-section and fluorescence yield of Sr also make
78 the experiment practicable. The Sr EXAFS-based
79 experiment requires PS II samples with Sr substituted
80 for Ca while maintaining O₂-evolving activity and a
81 stoichiometry of 1 Sr per PS II, to focus on the func-
82 tional cofactor binding site. Along with reactivated
83 Sr-PS II, an inactivated sample can be prepared by
84 treating with hydroxylamine (NH₂OH) to disrupt
85 the Mn cluster and suppress water oxidase activity
86 (Tamura and Cheniae, 1985).

87 By using Sr EXAFS on isotropic Sr-reactivated
88 PS II membranes, the proximity of Sr (and implicitly
89 Ca) to within 3.5 Å of the Mn cluster (Cinco et al.,
90 1998) has been confirmed. The finding was based on
91 the presence of a second Fourier peak (peak II, Fig.
92 9, *Top*) in the Sr EXAFS from functional samples,
93 a peak that is absent from inactive, hydroxylamine-
94 treated PS II. This Fourier peak was found to fit best
95 to two Mn at ~3.5 Å rather than lighter atoms (C, O,
96 P, S, Cl). Both types of samples share similar first
97 coordination shells of oxygen (Peak I, Fig. 9, *Top*).
98

2. Oriented Samples

99
100
101 The technique of using Sr EXAFS has been ex-
102 tended to using polarized Sr EXAFS on layered
103 Sr-substituted samples, to provide important angle
104

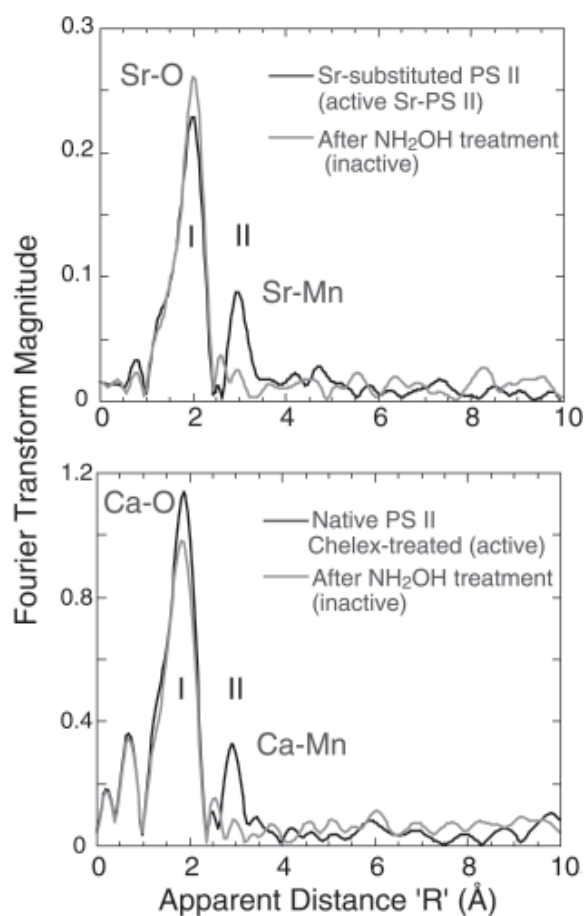


Fig. 9. Top. Fourier transforms of Sr EXAFS for intact and inactive Sr-substituted PS II samples (Chelex-treated). The dominant Fourier Peak I is due to ligating oxygens in the first coordination sphere and is common to both samples. The two Sr-PS II samples differ mainly at the 'R' = 3.0 Å region, where the intact samples exhibit Fourier Peak II. Disruption of the Mn cluster in NH₂OH-treated sample leads to the absence of Peak II. Bottom. Fourier Transform of Ca EXAFS from Chelex-treated, layered samples with 2 Ca/PS II with O₂-evolving activity and an S₂ EPR multiline signal. The FTs show the presence of a second Fourier peak in the 2Ca/PS II sample that fits to Ca-Mn that is absent in the control sample where the Mn complex has been disrupted with NH₂OH.

information. Polarized EXAFS involves collecting spectra for different incident angles (θ) between the membrane normal of the layered sample and the X-ray electric field vector. Dichroism in the EXAFS can occur, depending on how the particular absorber-backscatterer (A-B) vector is aligned with the electric field. Through analysis of the dichroism, the average orientation (ϕ) of this A-B vector relative to the membrane normal, and the average number of scatterers per absorbing atom (N_{iso}) can be extracted.

Constraints on the structural model are then imposed by these parameters.

Sr-substituted PS II samples made by a process of Ca depletion, Sr²⁺ reactivation, and Chelex treatment to remove excess Sr were layered onto flat Mylar films to produce oriented samples (Mukerji et al., 1994; Dau et al., 1995). The Fourier transforms from the polarized Sr EXAFS showed extreme dichroism in Fourier peak II (Fig. 10, Left). Nonlinear least-squares regression analysis produced the solid curve shown in Fig. 10, Right as the best fit of the 15 data points (angles from six separate samples) and the result translates to 1–2 Sr–Mn vectors with an average angle of 0° or 23° for the average relative angle between the Sr–Mn vectors and the membrane normal depending on the method of analysis.

3. Orientation of the Mn Complex

The orientation data from the Sr EXAFS experiments can be combined with the dichroism data from Mn EXAFS data to calculate the orientation of the 3.3 Å Mn–Mn vector. The Fourier peak in the Mn EXAFS which contains the Mn–Mn (3.3 Å) and Mn–Ca (3.4 Å) contributions, is dichroic, with an average angle of $43 \pm 10^\circ$ with respect to the membrane normal (Mukerji et al., 1994). By including the Mn–Ca vector at 23°, an angle of $\sim 62^\circ$ for the 3.3 Å Mn–Mn vector can be calculated. Previous polarized Mn EXAFS experiments on PS II have shown angles of 55° and 67° for the 2.7 Å Mn–Mn vectors (Mukerji et al., 1994; Dau et al., 1995). Thus it follows that all Mn–Mn vectors lie at roughly the same angle ($\sim 61^\circ$) with respect to the membrane normal, but are not restricted to being collinear, because the PS II membranes are ordered in one dimension only. The electron density from the X-ray diffraction studies (Zouni et al., 2001) are in agreement with such an assignment; the plane containing the Mn electron density is at $\sim 67^\circ$ to the membrane normal.

C. Ca Extended X-ray Absorption Fine Structure (EXAFS)

In a complementary and definitive experiment, Ca K-edge EXAFS studies have been used to probe the binding site of the native cofactor for any nearby Mn, within ~ 4 Å. The use of Ca EXAFS spectroscopy has produced results essentially congruent with those found by other independent methods: Sr EXAFS on Sr-reativated PS II (Cinco et al., 1998) and Mn

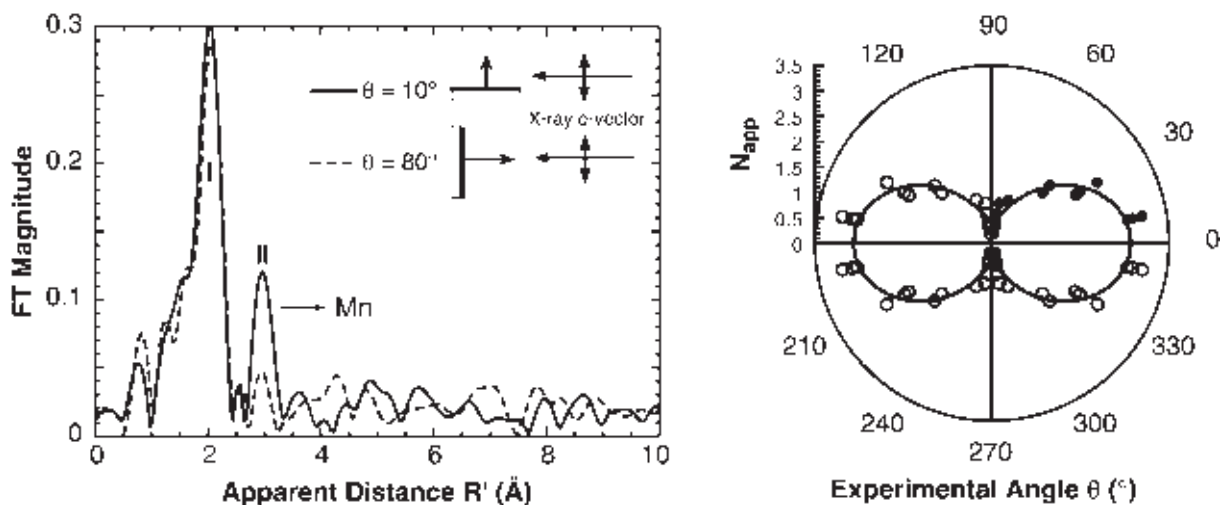


Fig. 10. *Left.* Fourier transforms of Sr-EXAFS from oriented Sr-PS II samples at two angles (θ). The dichroism is most readily apparent in Fourier peak II ($R' = 3.0$ Å) which is assigned to backscattering from Mn. *Right.* The polar plot shows N_{exp} (filled circles) plotted vs. the angle of detection, θ . The solid line is the best fit from which we obtain N_{iso} (number of Mn neighbors to Sr is ~ 2) and ϕ ($\sim 23^\circ$), the angle the Mn-Sr vector makes with the membrane normal.

EXAFS on similar samples (Latimer et al., 1995), but it focuses on the native cofactor and avoids the treatments involving Ca depletion and Sr substitution. Like the earlier Sr EXAFS, the Ca EXAFS study has focused on the Ca cofactor of PS II (poised in the S_1 state). This technique is a more sensitive and direct probe of the Ca binding site in PS II and the Ca EXAFS experiment directly probed the Ca cofactor in as close to a native system as possible.

The FT of the Ca EXAFS is shown in Fig. 9, *Bottom* and the spectra are remarkably similar to the Fourier transforms of the earlier Sr EXAFS study with Sr substituted for Ca. The first (largest) Fourier peak corresponds to the coordinating oxygen atoms closest to Ca. In contrast to the control (NH_2OH -treated) sample, the Chelex-treated PS II shows a second Fourier peak. When Fourier peak II is isolated and simulated with possible scattering atoms, it corresponded best to Mn at 3.4 Å, rather than to light atom (C, O or Cl) neighbors. These results were consistent with the earlier Sr EXAFS studies.

The results are summarized in a motif shown in Fig. 11 and this motif depicts the Ca linked to two Mn by single-O bridges, which can be supplied by protein residues or water. Only single-oxygen bridges (not bidentate bridges) can provide the required 3.4 Å distance indicated by the Ca EXAFS fitting. This bridge may be derived from carboxylate ligands (aspartate or glutamate protein residues), protein

backbone carboxyl, water or hydroxide.

Because significant information about Mn-Mn and Mn-Ca vector angles is now available, topological models previously discussed can be refined to include the presence of Ca and account for the dichroism data (Fig. 11). We have chosen to modify two options: option **F** (from Fig. 5) where the two di- μ -oxo motifs are formed using a common Mn atom and the mono- μ -oxo motif is placed at the end of the trinuclear unit, and option **G** can be thought of as at the corners of the base of a trigonal pyramid, with an O atom at the apex and three additional O atoms forming bridges pairwise among the Mn atoms below the base with the fourth Mn linked to one of the corner Mn atoms by a single O-atom bridge. Option **F** has two 2.7 to 2.8 Å Mn-Mn vectors while **G** has three such vectors. These structures are consistent with simulations of EPR and ENDOR data and also qualitatively in agreement with the reported electron density of the Mn cluster, especially the first option for **G** with Ca.

It has been speculated that Ca controls substrate water binding to the catalytic Mn site (Chen et al., 1995) and recent mechanisms have suggested the crucial involvement of the cofactor (Ananyev and Dismukes, 1997; Renger, 1997; Limburg et al., 1999; Siegbahn, 2000). The results Mn EXAFS, Sr EXAFS and Ca EXAFS are mutually consistent and converge toward the conclusion that the Ca co-

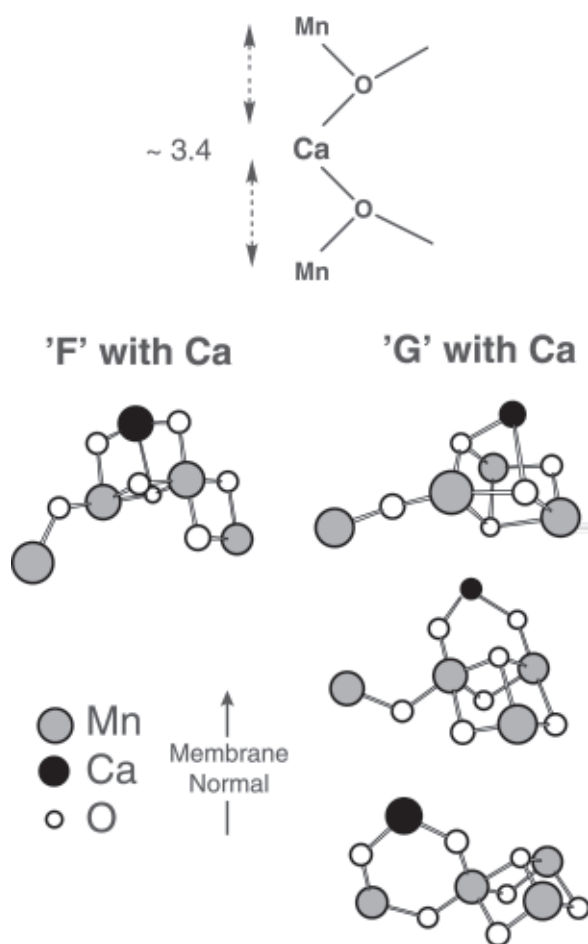


Fig. 11. Top. Model of Ca-binding site of the oxygen-evolving complex in PS II. From the results of the Ca EXAFS studies on PS II, the Ca cofactor is linked by two single-O bridges to two Mn. The oxygens can be provided by water, hydroxyl or protein residues (carboxylate, phenolate). Other ligands to Ca are not shown. The arrangement shown here is not unique as other placements of the two Mn around the Ca are conceivable (Cinco et al., 2002). *Bottom.* Refined models for the active site of the OEC in PS II. These models combine the finding from oriented Sr-substituted PS II samples with previous results from Mn EXAFS on oriented PS II samples. These are derived from core structures that have been described in earlier studies and the models presented here are based on options F and G from Fig. 5 (F with Ca is a variation on a model originally proposed by Siegbahn (2000).

factor is intimately structurally linked with the Mn cluster in PS II. Taken together, the three methods offer compelling evidence that the catalytic center of photosynthetic O₂ evolution is a heteronuclear Mn₄Ca cluster (for further details, see Chapter 21, Barber and Iwata).

V. Structural Role of the Chloride Cofactor

Despite a multitude of spectroscopic studies, definitive structural evidence for Mn-Cl ligation has not yet been reported. There is one functional Cl⁻ per PS II unit (Lindberg and Andréasson, 1996; Olesen and Andréasson, 2003), but it is unclear whether chloride is a ligand to one of the Mn atoms in any of the S-states (Lindberg et al., 1990). Steady-state kinetic studies indicate the presence of a halide binding site on the Mn complex (Sandusky and Yocum, 1986; Yocum, 1992; Lindberg and Andréasson, 1996) and activity is inhibited by some compounds which compete with the Cl⁻ binding site, such as fluoride (Sandusky and Yocum, 1986), primary amines (Sandusky and Yocum, 1986) and acetate (Clemens et al., 2002). Ono et al. (1986) have shown that Cl⁻ depleted PS II particles in the S₂ state do not have the usual multiline EPR signal but rather have a signal at g=4.1, signifying that an alternative S₂ state is formed. A similar EPR signal is observed on treatment with F⁻. It was found that when the OEC is in this alternative state, it can no longer advance to higher S-states. However, the EPR multiline signal is restored following illumination and subsequent addition of Cl⁻. Recent studies indicate that the presence of the Cl⁻ is necessary only for the S₂ to S₃ and S₃ to S₀ transitions of the OEC, while the earlier steps of the cycle can proceed in its absence (Wincencjusz et al., 1997, 1998). These studies indicate that Cl⁻ is closely associated with the structure of the OEC and the mechanism of O₂ evolution, but its detailed role is as yet unclear.

F⁻ perturbation of the Mn-Mn distances by treatment with F⁻ is one of the most direct structural data available that implies halide as a ligand of Mn. XAS studies of F⁻ inhibited samples show that one of the two 2.7 Å Mn-Mn distances is increased to ~2.8 Å, which is suggestive of F⁻ binding to the Mn cluster (DeRose et al., 1995). The recent ESEEM results from acetate treated PS II samples (Clemens et al., 2002) also provide the most direct spectroscopic evidence to date for the presence of a chloride ligand to Mn.

There is evidence from EXAFS studies with oriented S₃ state samples indicating the presence of Mn-Cl ligation in the S₃ state (Fernandez et al., 1998). EXAFS results from isotropic samples in the S₃ state have shown that there is considerable change in the Mn-Mn distances as the system advances from the S₂ to the S₃ state (Liang et al., 2000). The two 2.7 Å Mn-Mn distances in the S₂ state increase to ~2.8 and ~3.0 Å in the S₃ state. With the aim of determining the relative orientation of the 2.8 and

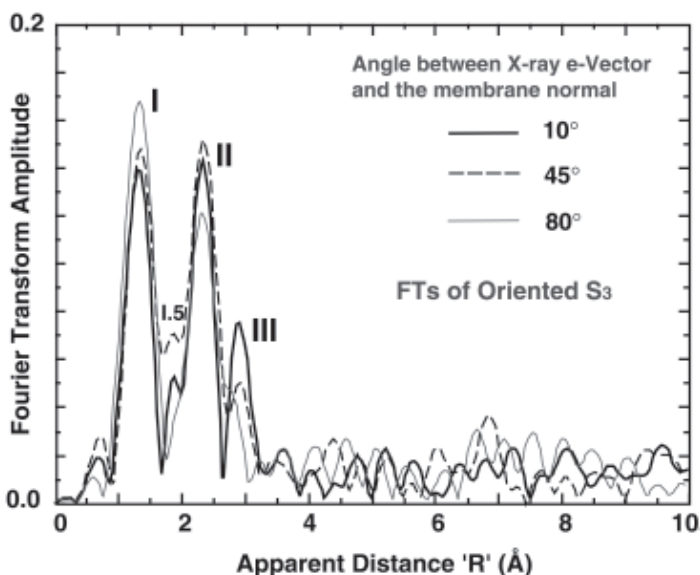


Fig. 12. The Fourier transform of an oriented S_3 sample. The Mn–Mn vectors represented by Fourier peaks labeled II and III are dichroic. Interestingly, a Fourier peak labeled 1.5 is discernible that is not observed in other S-states and it fits best to Cl, indicating the possible presence of a Cl ligand to Mn at a distance of 2.2 Å (Fernandez et al., 1998) in the S_3 state.

2.9–3.0 Å Mn–Mn vectors, we initiated XAS studies of oriented S_3 state samples. The FT in Fig. 12 shows that the two Mn–Mn vectors are dichroic. Interestingly, maybe because of the lengthening of the Mn–Mn vectors, a new Fourier peak is observed between the first and second Fourier peaks, labeled 1.5 in Fig. 12. Comparing this FT with that of a Mn binuclear complex with one Cl^- as a terminal ligand to a Mn atom shows that the peak corresponding to Cl backscattering in the model complex is found at approximately the same apparent distance as the new Fourier peak in the PS II samples (Fernandez et al., 1998). In other model compounds, the amplitude of this peak increases as the ratio of Cl/Mn increases and the peak is absent when Cl^- is not present as a ligand. In the S_3 state sample, this peak does not fit to lower Z atoms such as C, N, or O. The fit is significantly better for Cl backscattering at ~ 2.2 Å. The fits for the model compound are very similar. Dichroism studies on S_3 state samples show that the Fourier peak is larger at the 10° orientation compared to the 80° orientation, which suggests that the Mn–Cl vector is more parallel to the membrane normal.

VI. Mechanism of Water Oxidation and O_2 Evolution

The mechanisms for water oxidation and oxygen evolution that have been proposed can be broadly divided into four categories in which the character of the oxygen atoms that ultimately form dioxygen is different. In these four groups the oxygen atoms come from: two terminal oxygens bound to two separate Mn atoms, one terminal oxygen and one oxygen not bound to the Mn cluster, one terminal and one bridging oxygen, or two μ -oxo bridges. Each of these mechanisms involves distinctly different Mn–O bonds formed and broken during the catalytic cycle (see Chapter 25 for details).

The contribution of X-ray studies to the mechanism of O_2 evolution is in resolving whether an oxygen atom derived from a bridging position in the Mn cluster is involved in the ultimate formation of dioxygen and in the determination of whether Mn centered oxidation occurs during each stage of the S-state transitions. Our X-ray spectra are strongly supportive of Mn cluster oxidation during the $S_0 \rightarrow S_1$ and $S_1 \rightarrow S_2$ transitions, they do not support a similar Mn-centered oxidation during $S_2 \rightarrow S_3$. Furthermore, EXAFS analyses show clear evidence of non-degeneracy in the three 2.7 Å vector lengths in S_0 and S_3 , but not in S_1 and S_2 , and shows significant structural change

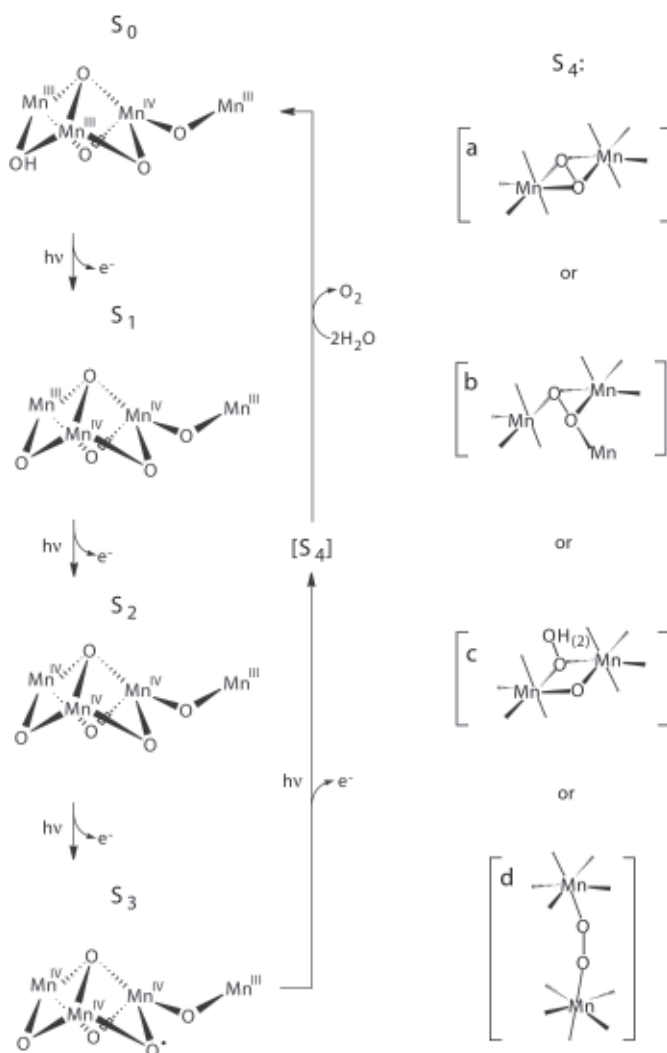


Fig. 13. Summary of changes in Mn oxidation states and Mn-Mn distances during photosynthetic water oxidation using option **G** in Fig. 5. In the $S_1 \rightarrow S_2$ transition, one Mn(III) is oxidized to Mn(IV), and the Mn-Mn distances do not change. During the $S_2 \rightarrow S_3$ transition, the oxidizing equivalent is localized on the μ -oxo bridge, which triggers the increase in Mn-Mn distances. In the $S_3 \rightarrow [S_4] \rightarrow S_0$ transition, a short-lived peroxo intermediate might be formed in the S_4 state. (a), (b), (c) and (d) are 4 mechanisms for O-O bond formation in the S_4 state. Mechanisms (a), (b) and (c) are where one or two bridging O atoms are directly involved in O-O bond formation; a motif that is consistent with XAS data. Mechanism (d) would require localization of an oxidizing equivalent on an oxo bridge that later exchanges or rearranges to a terminal O ligand before O-O bond formation. During the $S_0 \rightarrow S_1$ transition, a Mn(II) \rightarrow Mn(III) oxidation or a Mn(III) to Mn(IV) concurrent with a deprotonation of a hydroxy to an oxo causing the decrease of the Mn-Mn distance is indicated. For clarity, Y_Z , the cofactors Ca^{2+} and Cl^- , and terminal Mn ligands are not shown. Mn-Mn distances were determined by EXAFS spectroscopy. As mentioned in DeRose et al. (1994), Cinco et al. (2002) and Robblee et al. (2002) other possible topological models exist for the OEC; similar mechanisms that can be proposed for each of the alternative topological models should be considered equally viable.

during the S_2 to S_3 transition that is not accompanied by a Mn-centered oxidation. The X-ray spectroscopy evidence supports the involvement of a bridging O atom in the mechanism of the formation of the O-O bond. These observations must be considered in any postulation of mechanistic aspects of the successive

steps in water oxidation.

Our proposed mechanism (illustrated in Fig. 13 using the proposed model **G**) where the O-O bond is formed between one critical bridging oxygen and another oxygen atom derived from a bridging/terminal oxygen ligand or an exogenous oxygen also

1 avoids the formation of the O–O bond until the most
 2 oxidized state (S_4) is reached (Fig. 13, (a), (b), (c)).
 3 All four options for the S_4 state generate O_2 which
 4 is derived from inequivalent oxygen atoms in the S_3
 5 state, as shown by $^{16}O/^{18}O$ water-exchange measure-
 6 ments on the S_3 state (Messinger et al., 1995; Hillier
 7 et al., 1998). In addition, a recent $H_2^{16}O/H_2^{18}O$ FTIR
 8 experiment has shown the presence of an exchange-
 9 able di- μ -oxo-bridge in the S_1 and S_2 states (Chu et
 10 al., 2000). This mechanism precludes the formation
 11 and release of peroxide or other oxidation products
 12 of water in the earlier S-states, thus preventing the
 13 system from ‘short circuiting’ and avoiding the risk
 14 of damaging the polypeptides of PS II.

17 Acknowledgments

19 This work was supported by the National Institutes
 20 of Health grant (GM 55302) and by the Director,
 21 Office of Science, Office of Basic Energy Sciences,
 22 Division of Energy Biosciences, U. S. Department
 23 of Energy under contract DE-AC03-76SF00098. I
 24 am grateful to every one of the very talented and
 25 motivated graduate students and postdocs, and many
 26 sabbatical visitors to the Calvin Lab that I have had
 27 the privilege to work with on the oxygen evolving
 28 complex over the last two decades and more; each
 29 and every one of them can recognize some aspect of
 30 the work presented here that they were responsible for
 31 and that has contributed to the present understand-
 32 ing of the Mn cluster in the OEC. Specifically, the
 33 contributions to the research presented in this article
 34 by Roehl Cinco, John Robblee, Johannes Messinger,
 35 Henk Visser, Uwe Bergmann, Pieter Glatzel, Carmen
 36 Fernandez, Elodie Anxolabéhère-Mallart, Shelly
 37 Pizarro, Karen McFarlane, Junko Yano, Steve Cra-
 38 mer and Ken Sauer is gratefully acknowledged. Mel
 39 Klein’s profound influence and contributions to the
 40 EPR and X-ray spectroscopy research pervades the
 41 work presented in this chapter. I extend my thanks
 42 to our collaborators Profs. W. H. Armstrong, G. W.
 43 Brudvig, G. Christou, T. Collins, J.-J. Girerd, R. N.
 44 Mukherjee, V. L. Pecoraro and K. Wieghardt who
 45 have generously provided all the inorganic Mn com-
 46 pounds that has made all the difference in analyzing
 47 the data from PS II. Synchrotron radiation facilities
 48 were provided by the Stanford Synchrotron Radiation
 49 Laboratory (SSRL) and the Advanced Photon Source
 50 (APS), both supported by the U.S. Department of
 51 Energy and the National Institutes of Health.

References

- Adelroth P, Lindberg K and Andréasson LE (1995) Studies of Ca^{2+}
 binding in spinach Photosystem II using $^{45}Ca^{2+}$. *Biochemistry*
 34: 9021–9027
- Åhrling KA, Peterson S and Styring S (1998) The S_0 state EPR
 signal from the Mn cluster in Photosystem II arises from an
 isolated $S=1/2$ ground state. *Biochemistry* 37: 8115–8120
- Ananyev GM and Dismukes GC (1997) Calcium induces binding
 and formation of a spin-coupled dimanganese (II, II) center
 in the apo-water oxidation complex of Photosystem II as
 precursor to the functional tetra-Mn/Ca cluster. *Biochemistry*
 36: 11342–11350
- Auger N, Girerd J-J, Corbella M, Gleizes A and Zimmermann
 J-L (1990) Synthesis, structure, and magnetic properties of
 the stable triangular $[Mn(IV)_3O_4]^{4+}$ core. *J Am Chem Soc*
 112: 448–450
- Beck WF, Depaula JC and Brudvig GW (1986) Ammonia binds to
 the manganese site of the O_2 -evolving complex of Photosystem-
 II in the S_2 state. *J Am Chem Soc* 108: 4018–4022
- Bergmann U, Grush MM, Horne CR, DeMarois P, Penner-Hahn
 JE, Yocum CF, Wright DW, Dubé CE, Armstrong WH, Christou
 G, Eppley HJ and Cramer SP (1998) Characterization of the Mn
 oxidation states in Photosystem II by $K\beta$ X-ray fluorescence
 spectroscopy. *J Phys Chem B* 102: 8350–8352
- Boussac A and Rutherford AW (1988a) S-state formation after
 Ca^{2+} depletion in the Photosystem II oxygen-evolving complex.
Chem Script 28A: 123–126
- Boussac A and Rutherford AW (1988b) Nature of the inhibition
 of the oxygen-evolving enzyme of Photosystem II induced by
 NaCl washing and reversed by the addition of Ca^{2+} or Sr^{2+} .
Biochemistry 27: 3476–3483
- Boussac A and Rutherford AW (2000) Comparative study of the
 $g=4.1$ EPR signals in the S_2 state of Photosystem II. *Biochim*
Biophys Acta 1457: 145–156
- Boussac A, Girerd J-J and Rutherford AW (1996) Conversion of the
 spin state of the manganese complex in Photosystem II induced
 by near-infrared light. *Biochemistry* 35: 6984–6989
- Britt RD (1996) Oxygen evolution. In: Ort DR and Yocum CF (eds)
Oxygenic Photosynthesis: The Light Reactions, pp 137–164.
 Kluwer Academic Publishers, Dordrecht
- Britt RD, Zimmermann J-L, Sauer K and Klein MP (1989)
 Ammonia binds to the catalytic manganese of the oxygen-
 evolving complex of Photosystem II. Evidence by electron
 spin-echo envelope modulation spectroscopy. *J Am Chem*
Soc 111: 3522–3532
- Britt RD, Peloquin JM and Campbell KA (2000) Pulsed and par-
 allel-polarization EPR characterization of the Photosystem II
 oxygen-evolving complex. *Ann Rev Biophys Biomol Struct*
 29: 463–495
- Cammarata KV and Cheniae GM (1987) Studies on 17, 24
 kDa depleted Photosystem II membranes. *Plant Physiol* 84:
 587–595
- Carrell TG, Tyryshkin AM and Dismukes GC (2002) An evalua-
 tion of structural models for the photosynthetic water-oxidizing
 complex derived from spectroscopic and X-ray diffraction
 signatures. *J Biol Inorg Chem* 7: 2–22
- Chen C, Kazimir J and Cheniae GM (1995) Calcium modulates the
 photoassembly of Photosystem II (Mn) $_4$ -clusters by preventing
 ligation of nonfunctional high-valency states of manganese.

53
54
55
56
57
58
59
60
61
62
63
64
65
66
67
68
69
70
71
72
73
74
75
76
77
78
79
80
81
82
83
84
85
86
87
88
89
90
91
92
93
94
95
96
97
98
99
100
101
102
103
104

- 1 Biochemistry 34: 13511–13526
- 2 Chu H-A, Sackett H and Babcock GT (2000) Identification of
3 a Mn-O-Mn cluster vibrational mode of the oxygen-evolving
4 complex in Photosystem II by low-frequency FTIR spectroscopy. *Biochemistry* 39: 14371–14376
- 5 Cinco RM, Robblee JH, Rompel A, Fernandez C, Yachandra VK,
6 Sauer K and Klein MP (1998) Strontium EXAFS reveals the
7 proximity of calcium to the manganese cluster of oxygen-evolving
8 Photosystem II. *J Phys Chem B* 102: 8248–8256
- 9 Cinco RM, Rompel A, Visser H, Aromí G, Christou G, Sauer
10 K, Klein MP and Yachandra VK (1999) Comparison of the
11 manganese cluster in oxygen-evolving Photosystem II with
12 distorted cubane manganese compounds through X-ray absorption
13 spectroscopy. *Inorg Chem* 38: 5988–5998
- 14 Cinco RM, Holman KLM, Robblee JH, Yano J, Pizarro SA, Bel-
15 lacchio E, Sauer K and Yachandra VK (2002) Calcium EXAFS
16 establishes the Mn-Ca cluster in the oxygen-evolving complex
17 of Photosystem II. *Biochemistry* 41: 12928–12933
- 18 Clemens KL, Force DA and Britt RD (2002) Acetate binding at the
19 Photosystem II oxygen evolving complex: An S_2 -state multiline
20 signal ESEEM study. *J Am Chem Soc* 124: 10921–10933
- 21 Cole J, Yachandra VK, Guiles RD, McDermott AE, Britt RD,
22 Dexheimer SL, Sauer K and Klein MP (1987) Assignment of
23 the $g = 4.1$ EPR signal to manganese in the S_2 state of the photo-
24 synthetic oxygen-evolving complex: An X-ray absorption edge
25 spectroscopy study. *Biochim Biophys Acta* 890: 395–398
- 26 Cramer SP (1988) Biochemical application of X-ray absorp-
27 tion spectroscopy. In: Koningsberger DC and Prins R (eds)
28 X-Ray Absorption: Principles, Applications, Techniques of
29 EXAFS, SEXAFS and XANES, pp 327–320. John Wiley &
30 Sons, New York
- 31 Dau H, Andrews JC, Roelofs TA, Latimer MJ, Liang W, Yachandra
32 VK, Sauer K and Klein MP (1995) Structural consequences of
33 ammonia binding to the manganese cluster of the photosyn-
34 thetic oxygen-evolving complex: An X-ray absorption study of
35 isotropic and oriented Photosystem II particles. *Biochemistry*
36 34: 5274–5287
- 37 Debus RJ (1992) The manganese and calcium ions of photo-
38 synthetic oxygen evolution. *Biochim Biophys Acta* 1102:
39 269–352
- 40 Dekker JP (1992) Optical studies on the oxygen-evolving complex
41 of Photosystem II. In: Pecoraro VL (ed) *Manganese Redox*
42 *Enzymes*, pp 85–103. VCH Publishers, New York
- 43 DeRose VJ, Mukerji I, Latimer MJ, Yachandra VK, Sauer K and
44 Klein MP (1994) Comparison of the manganese oxygen-evolving
45 complex in Photosystem II of spinach and *Synechococcus*
46 sp. with multinuclear manganese model compounds by X-ray
47 absorption spectroscopy. *J Am Chem Soc* 116: 5239–5249
- 48 DeRose VJ, Latimer MJ, Zimmermann J-L, Mukerji I, Yachandra
49 VK, Sauer K and Klein MP (1995) Fluoride substitution in the
50 Mn cluster from Photosystem II: EPR and X-ray absorption
51 spectroscopy studies. *Chem Phys* 194: 443–459
- 52 Dismukes GC and Siderer Y (1981) Intermediates of a polynuclear
manganese cluster involved in photosynthetic oxidation of
water. *Proc Natl Acad Sci USA* 78: 274–278
- Evelo RG, Styring S, Rutherford AW and Hoff AJ (1989) EPR
relaxation measurements of Photosystem-II reaction centers
— influence of S-state oxidation and temperature. *Biochim
Biophys Acta* 973: 428–442
- Fernandez C, Cinco RM, Robblee JH, Messinger J, Pizarro SA,
Sauer K, Klein MP and Yachandra VK (1998) Calcium and
chloride cofactors of the oxygen evolving complex — X-ray
absorption spectroscopy evidence for a Mn/Ca/Cl heteronuclear
cluster. In: Garab G (ed) *Photosynthesis: Mechanisms and
Effects*, Vol II, pp 1399–1402. Kluwer Academic Publishers,
Dordrecht
- Ferreira K, Iverson TM, Mughlouni K, Barber J and Iwata S
(2004) Architecture of the photosynthetic oxygen-evolving
center. *Science* 303: 1831–1838
- George GN, Prince RC and Cramer SP (1989) The manganese
site of the photosynthetic water-splitting enzyme. *Science*
243: 789–791
- Ghanotakis DF, Babcock GT and Yocum CF (1984) Calcium
reconstitutes high rates of oxygen evolution in polypeptide
depleted Photosystem II preparations. *FEBS Lett* 167:
127–130
- Ghanotakis DF, Babcock GT and Yocum CF (1985) Structure of
the oxygen-evolving complex of Photosystem II: Calcium and
lanthanum compete for sites on the oxidizing side of Photosys-
tem II which control the binding of water-soluble polypeptides
and regulate the activity of the manganese complex. *Biochim
Biophys Acta* 809: 173–180
- Gilchrist ML, Jr., Ball JA, Randall DW and Britt RD (1995) Prox-
imity of the manganese cluster of Photosystem II to the redox-
active tyrosine Y_z . *Proc Natl Acad Sci USA* 92: 9545–9549
- Goodin DB, Yachandra VK, Britt RD, Sauer K and Klein MP
(1984) The state of manganese in the photosynthetic apparatus.
3. Light-induced changes in X-ray absorption (K-edge) energies
of manganese in photosynthetic membranes. *Biochim Biophys
Acta* 767: 209–216
- Guiles RD, Yachandra VK, McDermott AE, Cole JL, Dexheimer
SL, Britt RD, Sauer K and Klein MP (1990a) The S_0 state
of Photosystem II induced by hydroxylamine: Differences
between the structure of the manganese complex in the S_0
and S_1 states determined by X-ray absorption spectroscopy.
Biochemistry 29: 486–496
- Guiles RD, Zimmermann JL, McDermott AE, Yachandra VK, Cole
JL, Dexheimer SL, Britt RD, Wieghardt K, Bossek U, Sauer K
and Klein MP (1990b) The S_3 state of Photosystem II: Differ-
ences between the structure of the manganese complex in the
 S_2 and S_3 states determined by X-ray absorption-spectroscopy.
Biochemistry 29: 471–485
- Han K-C and Katoh S (1993) Different localization of two Ca^{2+} in
spinach oxygen-evolving Photosystem II membranes. Evidence
for involvement of only one Ca^{2+} in oxygen evolution. *Plant
Cell Physiol* 34: 585–593
- Hasegawa K, Kusunoki M, Inoue Y and Ono T-A (1998) Simula-
tion of S_2 -state multiline EPR signal in oriented Photosystem II
membranes: Structural implications for the manganese cluster in
an oxygen-evolving complex. *Biochemistry* 37: 9457–9465
- Hasegawa K, Ono T-A, Inoue Y and Kusunoki M (1999) Spin-
exchange interactions in the S_2 -state manganese tetramer in
photosynthetic oxygen-evolving complex deduced from $g=2$
multiline EPR signal. *Chem Phys Lett* 300: 9–19
- Hillier W, Messinger J and Wydrzynski T (1998) Kinetic determi-
nation of the fast exchanging substrate water molecule in the S_3
state of Photosystem II. *Biochemistry* 37: 16908–16914
- Iuzzolino L, Dittmer J, Dörner W, Meyer-Klaucke W and Dau H
(1998) X-ray absorption spectroscopy on layered Photosys-
tem II membrane particles suggests manganese-centered oxida-
tion of the oxygen-evolving complex for the S_0 - S_1 , S_1 - S_2 , and
 S_2 - S_3 transitions of the water oxidation cycle. *Biochemistry*

- 37: 17112–17119
- Jaklevic J, Kirby JA, Klein MP, Robertson AS, Brown GS and Eisenberger P (1977) Fluorescence detection of EXAFS: Sensitivity enhancement for dilute species and thin films. *Solid State Commun* 23: 679–682
- Joliot P (2003) Period-four oscillations of the flash-induced oxygen formation in photosynthesis. *Photosynth Res* 76: 65–72
- Kamiya N and Shen JR (2003) Crystal structure of oxygen-evolving Photosystem II from *Thermosynechococcus vulcanus* at 3.7 Å resolution. *Proc Natl Acad Sci USA* 100: 98–103
- Katoh S, Satoh K, Ohno T, Chen J-R and Kashino Y (1987) Numbers of calcium ions associated with oxygen evolving Photosystem II preparations with different affinities. In: Biggins J (ed) *Progress in Photosynthesis Research, Vol I*, pp 625–628. Martinus Nijhoff Publishers, Dordrecht
- Kirby JA, Robertson AS, Smith JP, Thompson AC, Cooper SR and Klein MP (1981) State of manganese in the photosynthetic apparatus. 1. Extended X-ray absorption fine structure studies on chloroplasts and di- μ -oxo-bridged dimanganese model compounds. *J Am Chem Soc* 103: 5529–5537
- Kok B, Forbush B and McGloin M (1970) Cooperation of charges in photosynthetic oxygen evolution. I. A linear four step mechanism. *Photochem Photobiol* 11: 457–475
- Kretschmann H, Dekker JP, Saygin Ö and Witt HT (1988) An agreement on the quaternary oscillation of ultraviolet absorption changes accompanying the water splitting in isolated Photosystem II complexes from the cyanobacterium *Synechococcus* sp. *Biochim Biophys Acta* 932: 358–361
- Kusunoki M, Takano T, Ono T, Noguchi T, Yamaguchi Y, Oyanagi H and Inoue Y (1995) Advanced EXAFS studies of the S₁ state manganese cluster in plant Photosystem II. In: Mathis P (ed) *Photosynthesis: From Light to Biosphere, Vol II*, pp 251–254. Kluwer Academic Publishers, Dordrecht
- Kuzek D and Pace RJ (2001) Probing the Mn oxidation states in the OEC Insights from spectroscopic, computational and kinetic data. *Biochim Biophys Acta* 1503: 123–137
- Lakshmi KV, Eaton SS, Eaton GR, Frank HA and Brudvig GW (1998) Analysis of dipolar and exchange interactions between manganese and tyrosine Z in the S₂Y_z state of acetate-inhibited Photosystem II via EPR spectral simulations at X- and Q-bands. *J Phys Chem B* 102: 8327–8335
- Latimer MJ, DeRose VJ, Mukerji I, Yachandra VK, Sauer K and Klein MP (1995) Evidence for the proximity of calcium to the manganese cluster of Photosystem II: Determination by X-ray absorption spectroscopy. *Biochemistry* 34: 10898–10909
- Latimer MJ, DeRose VJ, Yachandra VK, Sauer K and Klein MP (1998) Structural effects of calcium depletion on the manganese cluster of Photosystem II: Determination by X-ray absorption spectroscopy. *J Phys Chem B* 102: 8257–8265
- Liang W, Latimer MJ, Dau H, Roelofs TA, Yachandra VK, Sauer K and Klein MP (1994) Correlation between structure and magnetic spin state of the manganese cluster in the oxygen-evolving complex of Photosystem II in the S₂ state: Determination by X-ray absorption spectroscopy. *Biochemistry* 33: 4923–4932
- Liang W, Roelofs TA, Cinco RM, Rompel A, Latimer MJ, Yu WO, Sauer K, Klein MP and Yachandra VK (2000) Structural change of the Mn cluster during the S₂ → S₃ state transition of the oxygen-evolving complex of Photosystem II. Does it reflect the onset of water/substrate oxidation? Determination by Mn X-ray absorption spectroscopy. *J Am Chem Soc* 122: 3399–3412
- Limburg J, Szalai VA and Brudvig GW (1999) A mechanistic and structural model for the formation and reactivity of a Mn^v=O species in photosynthetic water oxidation. *J Chem Soc, Dalton Trans* 1353–1361
- Lindberg K and Andréasson LE (1996) A one-site, two-state model for the binding of anions in Photosystem II. *Biochemistry* 35: 14259–14267
- Lindberg K, Wydrzynski T, Vännegård T and Andréasson L-E (1990) Slow release of chloride from ³⁶Cl-labeled Photosystem II membranes. *FEBS Lett* 264: 153–155
- MacLachlan DJ, Hallahan BJ, Ruffle SV, Nugent JHA, Evans MCW, Strange RW and Hasnain SS (1992) An EXAFS study of the manganese oxygen-evolving complex in purified Photosystem II membrane fractions. The S₁ and S₂ states. *Biochem J* 285: 569–576
- MacLachlan DJ, Nugent JHA, Bratt PJ and Evans MCW (1994) The effects of calcium depletion on the O₂-evolving complex in spinach PS II: The S₁^{*}, S₂^{*} and S₃^{*} states and the role of the 17 kDa and 23 kDa extrinsic polypeptides. *Biochim Biophys Acta* 1186: 186–200
- McDermott AE, Yachandra VK, Guiles RD, Cole JL, Dexheimer SL, Britt RD, Sauer K and Klein MP (1988) Characterization of the manganese O₂-evolving complex and the iron-quinone acceptor complex in Photosystem II from a thermophilic cyanobacterium by electron paramagnetic resonance and X-ray absorption spectroscopy. *Biochemistry* 27: 4021–4031
- Messinger J, Badger M and Wydrzynski T (1995) Detection of one slowly exchanging substrate water molecule in the S₃ state of Photosystem II. *Proc Natl Acad Sci USA* 92: 3209–3213
- Messinger J, Nugent JHA and Evans MCW (1997a) Detection of an EPR multiline signal for the S₀^{*} state in Photosystem II. *Biochemistry* 36: 11055–11060
- Messinger J, Robblee J, Yu WO, Sauer K, Yachandra VK and Klein MP (1997b) The S₀ state of the oxygen-evolving complex in Photosystem II is paramagnetic: Detection of an EPR multiline signal. *J Am Chem Soc* 119: 11349–11350
- Messinger J, Robblee JH, Bergmann U, Fernandez C, Glatzel P, Visser H, Cinco RM, McFarlane KL, Bellacchio E, Pizarro SA, Cramer SP, Sauer K, Klein MP and Yachandra VK (2001) Absence of Mn-centered oxidation in the S₂ → S₃ transition: Implications for the mechanism of photosynthetic water oxidation. *J Am Chem Soc* 123: 7804–7820
- Mukerji I, Andrews JC, DeRose VJ, Latimer MJ, Yachandra VK, Sauer K and Klein MP (1994) Orientation of the oxygen-evolving manganese complex in a Photosystem II membrane preparation: An X-ray absorption spectroscopy study. *Biochemistry* 33: 9712–9721
- Olesen K and Andréasson LE (2003) The function of the chloride ion in photosynthetic oxygen evolution. *Biochemistry* 42: 2025–2035
- Ono T-A and Inoue Y (1988) Discrete extraction of the Ca atom functional for O₂ evolution in higher plant Photosystem II by a simple low pH treatment. *FEBS Lett* 227: 147–152
- Ono T-A and Inoue Y (1989) Roles of Ca²⁺ in O₂ evolution in higher plant Photosystem II: Effects of replacement of Ca²⁺ site by other cations. *Arch Biochem Biophys* 275: 440–448
- Ono T-A, Zimmermann JL, Inoue Y and Rutherford AW (1986) EPR evidence for a modified S-state transition in chloride-depleted Photosystem II. *Biochim. Biophys. Acta* 851: 193–201
- Ono T-A, Noguchi T, Inoue Y, Kusunoki M, Matsushita T and

- 1 Oyanagi H (1992) X-ray detection of the period-four cycling
2 of the manganese cluster in photosynthetic water oxidizing
3 enzyme. *Science* 258: 1335–1337
- 4 Ono T-A, Noguchi T, Inoue Y, Kusunoki M, Yamaguchi H and
5 Oyanagi H (1994) Study of the intermediate S-states for water
6 oxidation in the normal and Ca-depleted photosynthetic
7 oxygen-evolving enzyme by means of flash-induced X-ray
8 absorption near edge structure spectroscopy. *Biochem Soc
9 Trans* 22: 331–335
- 10 Pecoraro VL (ed) (1992) *Manganese Redox Enzymes*. VCH
11 Publishers, New York
- 12 Pecoraro VL and Hsieh W-Y (2000) The use of model complexes
13 to elucidate the structure and function of manganese redox
14 enzymes. In: Sigel A and Sigel H (eds) *Manganese and Its
15 Role in Biological Processes*, pp 429–504. Marcel Dekker
16 Inc., New York
- 17 Peloquin JM and Britt RD (2001) EPR/ENDOR characterization
18 of the physical and electronic structure of the OEC Mn cluster.
19 *Biochim Biophys Acta* 1503: 96–111
- 20 Peloquin JM, Campbell KA and Britt RD (1998) ^{55}Mn pulsed
21 ENDOR demonstrates that the Photosystem II ‘split’ EPR
22 signal arises from a magnetically-coupled manganese-tyrosyl
23 complex. *J Am Chem Soc* 120: 6840–6841
- 24 Peloquin JM, Campbell KA, Randall DW, Evanchik MA, Pecoraro
25 VL, Armstrong WH and Britt RD (2000) ^{55}Mn ENDOR of the
26 S_2 -state multiline EPR signal of Photosystem II: Implications
27 on the structure of the tetranuclear cluster. *J Am Chem Soc*
28 122: 10926–10942
- 29 Peng G, de Groot FMF, Hämäläinen K, Moore JA, Wang X,
30 Grush MM, Hastings JB, Siddons DP, Armstrong WH, Mullins
31 OC and Cramer SP (1994) High-resolution manganese X-ray
32 fluorescence spectroscopy. Oxidation-state and spin-state
33 sensitivity. *J Am Chem Soc* 116: 2914–2920
- 34 Penner-Hahn JE (1998) Structural characterization of the Mn
35 site in the photosynthetic oxygen-evolving complex. *Struct
36 Bond* 90: 1–36
- 37 Penner-Hahn JE, Fronko RM, Pecoraro VL, Yocum CF, Betts
38 SD and Bowlby NR (1990) Structural characterization of
39 the manganese sites in the photosynthetic oxygen-evolving
40 complex using X-ray absorption- spectroscopy. *J Am Chem
41 Soc* 112: 2549–2557
- 42 Renger G (1997) Mechanistic and structural aspects of photosyn-
43 thetic water oxidation. *Physiol Plant* 100: 828–841
- 44 Riggs PJ, Yocum CF, Penner-Hahn JE and Mei R (1992) Reduced
45 derivatives of the manganese cluster in the photosynthetic oxy-
46 gen-evolving complex. *J Am Chem Soc* 114: 10650–10651
- 47 Riggs-Gelasco PJ, Mei R, Yocum CF and Penner-Hahn JE (1996a)
48 Reduced derivatives of the Mn cluster in the oxygen-evolving
49 complex of Photosystem II: An EXAFS study. *J Am Chem
50 Soc* 118: 2387–2399
- 51 Riggs-Gelasco PJ, Mei R, Ghanotakis DF, Yocum CF and Penner-
52 Hahn JE (1996b) X-ray absorption spectroscopy of calcium-
substituted derivatives of the oxygen-evolving complex of
Photosystem II. *J Am Chem Soc* 118: 2400–2410
- Robblee JH, Cinco RM and Yachandra VK (2001) X-ray spec-
troscopy-based structure of the Mn cluster and mechanism
of photosynthetic oxygen evolution. *Biochim Biophys Acta*
1503: 7–23
- Robblee JH, Messinger J, Cinco RM, McFarlane KL, Fernandez
C, Pizarro SA, Sauer K and Yachandra VK (2002) The Mn
cluster in the S_0 state of the oxygen-evolving complex of
Photosystem II studied by EXAFS spectroscopy: Are there
three di- μ -oxo-bridged Mn_2 moieties in the tetranuclear Mn
complex? *J Am Chem Soc* 124: 7459–7471
- Roe AL, Schneider DJ, Mayer RJ, Pyrz JW, Widom J and Que
L, Jr (1984) X-ray absorption spectroscopy of iron-tyrosinate
proteins. *J Am Chem Soc* 106: 1676–1681
- Roelofs TA, Liang W, Latimer MJ, Cinco RM, Rompel A, Andrews
JC, Sauer K, Yachandra VK and Klein M (1996) Oxidation
states of the manganese cluster during the flash-induced S-state
cycle of the photosynthetic oxygen-evolving complex. *Proc
Natl Acad Sci USA* 93: 3335–3340
- Rutherford AW, Zimmermann J-L and Boussac A (1992) Oxy-
gen evolution. In: Barber J (ed) *The Photosystems: Structure,
Function, and Molecular Biology*, pp 179–229. Elsevier B.
V., Amsterdam
- Sandusky PO and Yocum CF (1986) The chloride requirement for
photosynthetic oxygen evolution: Factors affecting nucleophilic
displacement of chloride from the oxygen-evolving complex.
Biochim Biophys Acta 849: 85–93
- Sauer K, Yachandra VK, Britt RD and Klein MP (1992) The
photosynthetic water oxidation complex studied by EPR and
X-ray absorption spectroscopy. In: Pecoraro VL (ed) *Manganese
Redox Enzymes*, pp 141–175. VCH Publishers, New York
- Sayers DE, Stern EA and Lytle F (1971) New technique for
investigating noncrystalline structures. Fourier analysis of
the extended X-ray-absorption fine structure. *Phys Rev Lett*
27: 1204–1207
- Saygin Ö and Witt HT (1987) Optical characterization of inter-
mediates in the water-splitting enzyme system of photosyn-
thesis—possible states and configurations of manganese and
water. *Biochim Biophys Acta* 893: 452–469
- Schiller H, Dittmer J, Iuzzolino L, Dörner W, Meyer-Klaucke W,
Solé VA, Nolting H-F and Dau H (1998) Structure and orien-
tation of the oxygen-evolving manganese complex of green
algae and higher plants investigated by X-ray absorption linear
dichroism spectroscopy on oriented Photosystem II membrane
particles. *Biochemistry*: 37: 7340–7350
- Sharp RR (1992) Proton NMR relaxation due to the photosynthetic
oxygen-evolving center. In: Pecoraro VL (ed) *Manganese Redox
Enzymes*, pp 177–196. VCH Publishers, New York
- Shen J-R, Satoh K and Katoh S (1988) Calcium content of
oxygen-evolving Photosystem II preparations from higher
plants. Effects of NaCl treatment. *Biochim Biophys Acta*
933: 358–364
- Shulman RG, Yafet Y, Eisenberger P and Blumberg WE (1976)
Observation and interpretation of X-ray absorption edges in
iron compounds and proteins. *Proc Natl Acad Sci USA* 73:
1384–1388
- Siegbahn PEM (2000) Theoretical models for the oxygen radi-
cal mechanism of water oxidation and of the water oxidizing
complex of Photosystem II. *Inorg Chem* 39: 2923–2935
- Sivaraja M, Tso J and Dismukes GC (1989) A calcium-specific site
influences the structure and activity of the manganese cluster
responsible for photosynthetic water oxidation. *Biochemistry*
28: 9459–9464
- Smith PJ and Pace RJ (1996) Evidence for two forms of the
 $g=4.1$ signal in the S_2 state of Photosystem II. Two magne-
tically isolated manganese dimers. *Biochim Biophys Acta* 1275:
213–220
- Styring SA and Rutherford AW (1988) The microwave power satu-
ration of S_{IIslow} varies with the redox state of the oxygen-evolving

1	complex in Photosystem II. <i>Biochemistry</i> 27: 4915–4923	53
2	Tamura N and Chenuae G (1985) Effects of Photosystem-II	54
3	extrinsic proteins on microstructure of the oxygen-evolving	55
4	complex and its reactivity to water analogs. <i>Biochim Biophys</i>	56
5	<i>Acta</i> 809: 245–259	57
6	Tsutsumi K, Nakamori H and Ichikawa K (1976) X-ray manganese	58
7	K β emission spectra of manganese oxides and manganates.	59
8	<i>Phys Rev B</i> 13: 929–933	60
9	Visser H, Anxolabéhère-Mallart E, Bergman U, Glatzel P, Robblee	61
10	JH, Cramer SP, Girerd J-J, Sauer K, Klein MP and Yachandra	62
11	VK (2001) Mn K-edge XANES and K β XES studies of two	63
12	Mn-oxo binuclear complexes. Investigation of three different	64
13	oxidation states relevant to the oxygen-evolving complex of	65
14	Photosystem II. <i>J Am Chem Soc</i> 123: 7031–7039	66
15	Westre TE, Kennepohl P, DeWitt JG, Hedman B, Hodgson KO	67
16	and Solomon EI (1997) A multiplet analysis of Fe K-edge 1s	68
17	to 3d pre-edge features of iron complexes. <i>J Am Chem Soc</i>	69
18	119: 6297–6314	70
19	Wieghardt K (1989) The active centers in manganese-containing	71
20	metalloproteins and inorganic model complexes. <i>Angew Chem</i>	72
21	<i>Int Ed Engl</i> 28: 1153–1172	73
22	Wincencjusz H, van Gorkom HJ and Yocum CF (1997) The pho-	74
23	tosynthetic oxygen evolving complex requires chloride for its	75
24	redox state S ₂ to S ₃ and S ₃ to S ₀ transitions but not for S ₀ to S ₁	76
25	or S ₁ to S ₂ transitions. <i>Biochemistry</i> 36: 3663–3670	77
26	Wincencjusz H, Yocum CF and van Gorkom HJ (1998) S-state	78
27	dependence of chloride binding affinities and exchange dynam-	79
28	ics in the intact and polypeptide-depleted O ₂ evolving complex	80
29	of Photosystem II. <i>Biochemistry</i> 37: 8595–8604	81
30	Yachandra VK (1995) X-ray absorption spectroscopy and applica-	82
31	tions in structural biology. In: Sauer K (ed) <i>Methods of Enzy-</i>	83
32	<i>mology</i> , Vol 246, pp 638–675. Academic Press, San Diego	84
33	Yachandra VK (2002) Structure of the manganese complex in	85
34	Photosystem II: Insights from X-ray spectroscopy. <i>Phil Trans</i>	86
35	<i>R Soc London B</i> 357: 1347–1357	87
36		88
37		89
38		90
39		91
40		92
41		93
42		94
43		95
44		96
45		97
46		98
47		99
48		100
49		101
50		102
51		103
52		104